6 The LDA+DMFT Approach

Eva Pavarini
Institute for Advanced Simulation
Forschungszentrum Jülich GmbH

Contents

Eva Pavarini, Erik Koch, Dieter Vollhardt, and Alexander Lichtenstein (eds.)
The LDA+DMFT approach to strongly correlated materials
Forschungszentrum Jülich 2011, ISBN 978-3-89336-734-4

It would indeed be remarkable if Nature fortified herself against further advances in knowledge behind the analytical difficulties of the many-body problem. (Max Born, 1960)

1 The many-body problem

Most of chemistry and solid-state physics is described by the Hamiltonian

$$\hat{H} = -\frac{1}{2}\sum_i \nabla_i^2 + \frac{1}{2}\sum_{i\neq i'} \frac{1}{|\mathbf{r}_i - \mathbf{r}_{i'}|} - \sum_{i,\alpha} \frac{Z_\alpha}{|\mathbf{r}_i - \mathbf{R}_\alpha|} - \sum_\alpha \frac{1}{2M_\alpha}\nabla_\alpha^2 + \frac{1}{2}\sum_{\alpha\neq\alpha'} \frac{Z_\alpha Z_{\alpha'}}{|\mathbf{R}_\alpha - \mathbf{R}_{\alpha'}|},$$

where $\{\mathbf{r}_i\}$ are the coordinates of the N_e electrons, $\{\mathbf{R}_\alpha\}$ those of the N_n nuclei, Z_α the atomic numbers, and M_α the nuclear masses. The Born-Oppenheimer product Ansatz $\Psi(\{\mathbf{r}_i\},\{\mathbf{R}_\alpha\}) = \psi(\{\mathbf{r}_i\};\{\mathbf{R}_\alpha\})\Phi(\{\mathbf{R}_\alpha\})$ simplifies the problem. The Schrödinger equation for the electrons, $H_e\psi = \varepsilon\psi$, with

$$\begin{aligned}\hat{H}_e &= -\frac{1}{2}\sum_i \nabla_i^2 + \frac{1}{2}\sum_{i\neq i'} \frac{1}{|\mathbf{r}_i - \mathbf{r}_{i'}|} - \sum_{i\alpha} \frac{Z_\alpha}{|\mathbf{r}_i - \mathbf{R}_\alpha|} + \frac{1}{2}\sum_{\alpha\neq\alpha'} \frac{Z_\alpha Z_{\alpha'}}{|\mathbf{R}_\alpha - \mathbf{R}_{\alpha'}|} \\ &= \hat{T}_e + \hat{V}_{ee} + \hat{V}_{en} + \hat{V}_{nn}, \end{aligned} \tag{1}$$

has however a simple solution only in the non-interacting limit ($\hat{V}_{ee} = 0$). In this case, H_e is separable as $\hat{H}_e = \sum_i \hat{h}_e^0(\mathbf{r}_i) + \hat{V}_{nn}$, with

$$\hat{h}_e^0(\mathbf{r}) = -\frac{1}{2}\nabla^2 - \sum_\alpha \frac{Z_\alpha}{|\mathbf{r} - \mathbf{R}_\alpha|} = -\frac{1}{2}\nabla^2 + v_{\rm ext}(\mathbf{r}).$$

In a crystal the external potential $v_{\rm ext}(\mathbf{r})$ is periodic, the eigenvectors of $\hat{h}_e^0(\mathbf{r})$ are Bloch functions, $\psi_{n\mathbf{k}\sigma}(\mathbf{r})$. The eigenvalues are the corresponding band energies, $\varepsilon_{n\mathbf{k}}$. Many-electron ($N_e > 1$) states may be obtained by filling energy levels $\varepsilon_{n\mathbf{k}}$ with electrons and anti-symmetrizing the wave-function according to the Pauli principle (Slater determinant). For a half-filled band described by the dispersion relation $\varepsilon_{\mathbf{k}}$, such a Slater determinant has the form

$$\psi(\{\mathbf{r}_i\};\{\mathbf{R}_\alpha\}) = \frac{1}{\sqrt{N_e!}} \begin{vmatrix} \psi_{\mathbf{k}_1\uparrow}(\mathbf{r}_1) & \psi_{\mathbf{k}_1\uparrow}(\mathbf{r}_2) & \dots & \psi_{\mathbf{k}_1\uparrow}(\mathbf{r}_{N_e}) \\ \psi_{\mathbf{k}_1\downarrow}(\mathbf{r}_1) & \psi_{\mathbf{k}_1\downarrow}(\mathbf{r}_2) & \dots & \psi_{\mathbf{k}_1\downarrow}(\mathbf{r}_{N_e}) \\ \vdots & \vdots & \vdots & \vdots \\ \psi_{\mathbf{k}_{\frac{N_e}{2}}\uparrow}(\mathbf{r}_1) & \psi_{\mathbf{k}_{\frac{N_e}{2}}\uparrow}(\mathbf{r}_2) & \dots & \psi_{\mathbf{k}_{\frac{N_e}{2}}\uparrow}(\mathbf{r}_{N_e}) \\ \psi_{\mathbf{k}_{\frac{N_e}{2}}\downarrow}(\mathbf{r}_1) & \psi_{\mathbf{k}_{\frac{N_e}{2}}\downarrow}(\mathbf{r}_2) & \dots & \psi_{\mathbf{k}_{\frac{N_e}{2}}\downarrow}(\mathbf{r}_{N_e}) \end{vmatrix}. \tag{2}$$

Unfortunately, the electron-electron repulsion is strong, and the non-interacting electrons approximation is insufficient to understand real materials. Because $\hat{V}_{ee}$ is not separable, with increasing N_e, finding the solution of the Schrödinger equation $H_e\psi = \varepsilon\psi$ becomes quickly an unfeasible task, even for a single atom.

A big step forward was the development of density-functional theory (DFT) [1,2], described in detail in the Lecture of Peter Blöchl. DFT is based on the Hohenberg-Kohn theorem, which

establishes the one-to-one correspondence between the ground-state electron density $n(\mathbf{r})$ of an interacting system and the external potential $v_{\rm ext}(\mathbf{r})$ acting on it. For any material described by the Hamiltonian (1), the ground-state total energy is a functional of the electron density, $E[n]$, which is minimized by the ground-state density. $E[n]$ can be written as

$$E[n] = F[n] + \int d\mathbf{r}\; v_{ext}(\mathbf{r}) n(\mathbf{r}) + E_{nn} = F[n] + V[n] + E_{nn}.$$

$F[n] = T_e[n] + E_{ee}[n]$, the sum of the kinetic and electron-electron interaction energy, is a (unknown) universal functional (the same for all systems). $V[n]$ is the system-specific potential energy. The shift E_{nn} is the nucleus-nucleus interaction energy. The obstacle is that finding $n(\mathbf{r})$ still requires, in principle, the solution of the many-body problem (1). Kohn and Sham have shown, however, that $n(\mathbf{r})$ can be obtained by solving the Schrödinger equation of a fictitious non-interacting system, whose external potential $v_R(\mathbf{r})$ is chosen such that the ground-state density $n_0(\mathbf{r})$ equals $n(\mathbf{r})$

$$n(\mathbf{r}) = n_0(\mathbf{r}) = \sum_n^{\rm occ} |\psi_n(\mathbf{r})|^2.$$

To obtain the Hamiltonian $\hat{h}_e^0(\mathbf{r})$ of such an auxiliary problem we rewrite $F[n]$ as

$$F[n] = T_0[n] + E_H[n] + E_{xc}[n] = T_0[n] + \frac{1}{2}\int d\mathbf{r} \int d\mathbf{r}'\; \frac{n(\mathbf{r})n(\mathbf{r}')}{|\mathbf{r}-\mathbf{r}'|} + E_{xc}[n],$$

where $T_0[n]$ is the kinetic energy of the auxiliary system, $E_H[n]$ the classical electrostatic (or Hartree) energy, and $E_{xc}[n]$ is the small exchange-correlation correction,

$$E_{xc}[n] = E_{ee}[n] - E_H[n] + T_e[n] - T_0[n].$$

By minimizing the total energy with respect to $\{\psi_n\}$, with the constraint $\langle\psi_n|\psi_{n'}\rangle = \delta_{n,n'}$, we find the Kohn-Sham equation

$$\hat{h}_e^0(\mathbf{r})\; \psi_n(\mathbf{r}) = [-\frac{1}{2}\nabla^2 + v_{\rm R}(\mathbf{r})]\psi_n(\mathbf{r}) = \varepsilon_n \psi_n(\mathbf{r}). \tag{3}$$

The eigenvalues ε_n are the Lagrange multipliers which enter the minimization through the constraint. The external (or reference) potential is given by

$$v_{\rm R}(\mathbf{r}) = -\sum_\alpha \frac{Z_\alpha}{|\mathbf{r}-\mathbf{R}_\alpha|} + \int d\mathbf{r}' \frac{n(\mathbf{r}')}{|\mathbf{r}-\mathbf{r}'|} + \frac{\delta E_{xc}[n]}{\delta n}.$$

The exchange-correlation functional is unknown, and includes a Coulomb ($E_{ee}[n] - E_H[n]$) and a kinetic energy ($T_e[n] - T_0[n]$) term. The latter can be transformed into a correction of the Coulomb term by means of a coupling-constant integration: The interaction V_{ee} is rescaled by a parameter λ (with $0 \le \lambda \le 1$), while keeping $n(\mathbf{r})$ fixed; this constraint is fulfilled through a reference potential $v_R^\lambda(\mathbf{r})$. Using the Hellmann-Feynman theorem to calculate $\frac{\partial E_\lambda}{\partial \lambda}$, where $E_\lambda = \langle\Psi_\lambda|H_\lambda|\Psi_\lambda\rangle$ is the ground-state energy at coupling constant λ, and then integrating over λ to obtain $E_1 - E_0$, one may show that

$$E_{xc}[n] = \int d\mathbf{r} \int d\mathbf{r}'\; \frac{n(\mathbf{r})n(\mathbf{r}')(\overline{g}(\mathbf{r},\mathbf{r}')-1)}{|\mathbf{r}-\mathbf{r}'|},$$

where

$$\overline{g}(\mathbf{r},\mathbf{r}') = \int_0^1 d\lambda\, g_\lambda(\mathbf{r},\mathbf{r}').$$

The quantity $n(\mathbf{r},\mathbf{r}') = \sum_{\sigma,\sigma'} n(\mathbf{r}\sigma,\mathbf{r}'\sigma') = n(\mathbf{r}')n(\mathbf{r})g_\lambda(\mathbf{r},\mathbf{r}')$ is the joint probability of finding electrons at $\mathbf{r}$ and $\mathbf{r}'$. The function $g_\lambda(\mathbf{r},\mathbf{r}')$ is the pair-correlation function. It can be shown that $g_\lambda(\mathbf{r},\mathbf{r}') - 1$ vanishes in the large $|\mathbf{r}-\mathbf{r}'|$ limit.
In the Hartree-Fock approximation, in which the wavefunction is a Slater determinant, e.g. (2)

$$n(\mathbf{r}\sigma,\mathbf{r}'\sigma') = n(\mathbf{r}\sigma)n(\mathbf{r}'\sigma') - \delta_{\sigma,\sigma'}\left|\sum_i^{N_e/2} \overline{\psi}_{\mathbf{k}_i\sigma}(\mathbf{r})\psi_{\mathbf{k}_i\sigma}(\mathbf{r}')\right|^2, \tag{4}$$

where the last term accounts for the Pauli exclusion principle (*exchange*) and cancels the unphysical interaction of each electron with itself (*self-interaction*) present in the Hartree energy. The following sum rule holds for the pair-correlation function

$$\int d\mathbf{r}'\, n(\mathbf{r}')(g_\lambda(\mathbf{r},\mathbf{r}') - 1) = -1. \tag{5}$$

This -1 is, in atomic units (Appendix A), a positive charge $-e$. The exchange-correlation energy $E_{xc}[n]$ may thus be interpreted as the energy gain due to the interaction of each electron with an *exchange-correlation hole* with charge density $n(\mathbf{r}')(g_\lambda(\mathbf{r},\mathbf{r}')-1)$ surrounding it. Since the *exchange hole* described by Eq. (4) already satisfy the sum rule (5), the remaining *correlation hole* redistributes the charge density of the hole. In the one-electron case ($N_e = 1$), $E_{xc}[n]$ merely cancels the Hartree self-interaction energy.
The main difficulty of DFT is to find good approximations to $E_{xc}[n]$. The most common is the local-density approximation (LDA), in which $E_{xc}[n]$ is replaced by its expression for a homogeneous interacting electron gas with density equal to the local density $n(\mathbf{r})$

$$E_{xc}[n] = \int d\mathbf{r}\epsilon_{xc}^{\rm LDA}(n(\mathbf{r}))n(\mathbf{r}). \tag{6}$$

The LDA is particularly justified in systems with slowly varying spatial density $n(\mathbf{r})$. For such materials, we could split space into regions in which the density is basically constant and the system can indeed be described by a homogeneous electron gas; if we add up the contributions of all these regions of space we obtain the integral (6). The spin-polarized extension of the local-density approximation is the local spin-density approximation (LSDA).
The ground-state electron-density $n(\mathbf{r})$ can be obtained by solving (3) self-consistently. Various successful methods have been developed to find the eigenvalues and eigenvectors of (3), for solids and molecules. They are based on atomic-like orbitals (LMTO, NMTO), plane-waves (pseudopotentials), combinations of both (LAPW, PAW), gaussians, or Green functions (KKR) [3]. Through the years, DFT and the LDA have provided insight not only in solid-state physics, but also in chemistry and even in systems of biological interest. For this reason DFT became the *standard model* for electronic-structure calculations [1–3]. Strictly speaking, the Kohn-Sham energies ε_n have no physical meaning except the highest occupied state, which

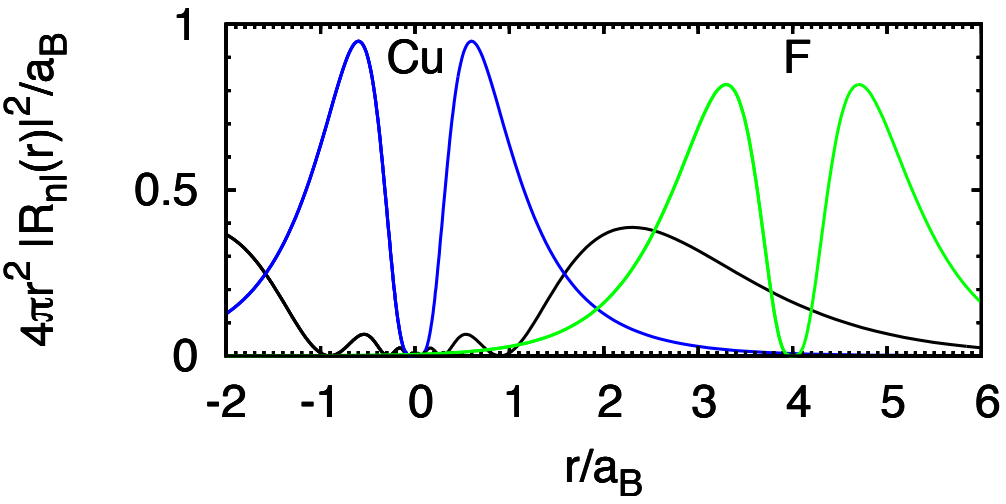

Fig. 1: *LDA solution of the Schrödinger equation for a single atom:* $4\pi r^2 |R_{nl}(r)|^2/a_B$ *as a function of the distance from the nucleus,* r/a_B *(atomic units, Appendix A). Blue: Cu* $3d$*. Black: Cu* $4s$*. The* $2p$ *orbital of a F atom in* $r = 4a_B$ *is also shown (green). Cu has the electronic configuration [Ar]* $3d^{10}4s^1$ *and F the configuration [He]* $2s^2 2p^5$*.*

yields the ionization energy, and their identification with one-particle energies is not justified. The Kohn-Sham orbitals $\psi_n(\mathbf{r})$ are just a tool to generate the ground-state density $n(\mathbf{r})$. Nevertheless, in practice Kohn-Sham orbitals turned out to be very useful to explain the properties of solids. Fermi surfaces, chemistry and many features of the electronic structure are qualitatively and often quantitatively well described by DFT in the LDA approximation or its extensions. The energy gap of semiconductors is underestimated, but can be corrected within many-body perturbation theory (GW approximation, discussed in the Lecture of Karsten Held).

LDA fails to capture, however, the essential physics of *strongly-correlated systems*, even at a qualitative level. At the center of this discrepancy are many-body effects between electrons in open d or f shells. Since these electrons are very *localized*, the Coulomb repulsion between them is significant. When Coulomb repulsion is strong, electrons lose their individuality: The dynamics of a single electron depends on the position of all others, the Coulomb repulsion of which it has to avoid (electrons are strongly correlated), and cannot be described by a reference mean-field potential. This happens for example in the case of *Mott insulators*. Because the Kohn-Sham Hamiltonian (3) with the LDA exchange-correlation potential describes independent electrons, many-electron states can be built from the Kohn-Sham orbitals as a single Slater determinant. Thus, a non-magnetic crystal with an odd number of electrons per unit cell has partially filled bands because of spin degeneracy, and therefore is metallic. However, due to Coulomb repulsion, several transition-metal compounds with partially filled d shells are insulating, paramagnetic above the Neel temperature T_N, and sometimes exhibit a large gap. In Fig. 1 the extensions of the atomic radial functions for the outer orbitals, $3d$ and $4s$, of Cu can be compared. While for $3d$ electrons the radial function decays very rapidly with distance, for

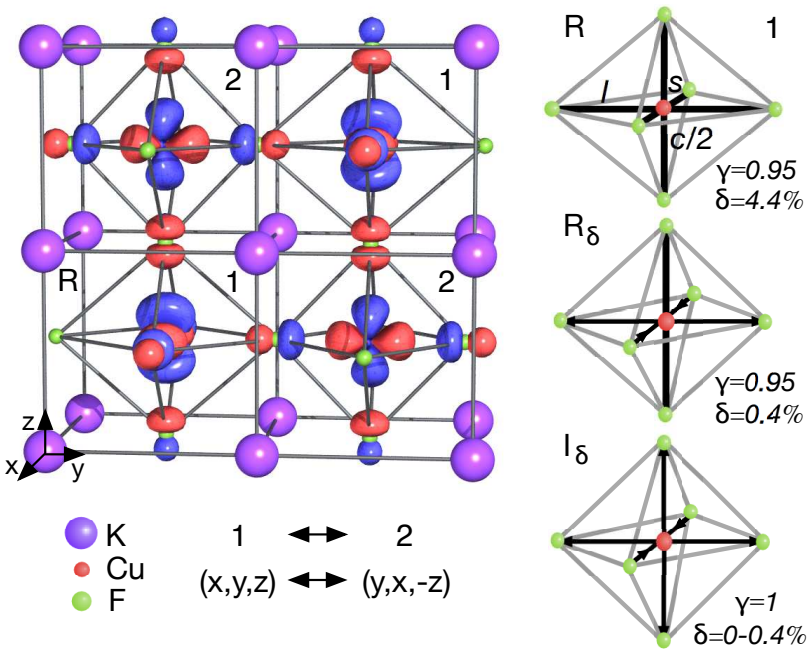

Fig. 2: *Crystal structure, distortions and orbital order in $KCuF_3$. Cu is at the center of F octahedra enclosed in a K cage. The conventional cell is tetragonal with axes* $\mathbf{a}$, $\mathbf{b}$, $\mathbf{c}$. *The pseudocubic axes* $\mathbf{x}$, $\mathbf{y}$, $\mathbf{z}$ *pointing towards neighboring Cu are shown in the corner. Short (s) and long (l) CuF bonds alternate between* $\mathbf{x}$ *and* $\mathbf{y}$ *along all pseudocubic axes (co-operative Jahn-Teller distortion). The distortions are measured by* $\delta = (l-s)/(l+s)/2$ *and* $\gamma = c/a\sqrt{2}$. *R is the experimental structure ($\gamma = 0.95$, $\delta = 4.4\%$), R_δ ($\gamma = 0.95$) and I_δ ($\gamma = 1$) two ideal structures with reduced distortions. In the I_0 structure the cubic crystal-field at the Cu site splits the 3d manifold into a t_{2g} triplet and a e_g doublet. In the R structure, site symmetry is lowered further by the tetragonal compression ($\gamma < 1$) and the Jahn-Teller distortion ($\delta \neq 0$). The figure shows the highest energy d orbital. From Ref. [4].*

$4s$ electrons it is still sizable ~ 2 Å away from the nucleus, a typical interatomic distance in a lattice. Thus in a crystal $4s$ electrons are likely to form delocalized states, while $3d$ electrons tend to retain part of their atomic characteristics.

As example we take $KCuF_3$. This system has a perovskite structure, shown in Fig. 2, with each Cu surrounded by a F octahedron. The nominal valence for K, Cu and F is K^+ ($4s^0$), F^- ($2p^6$), Cu^{2+} ($3d^9 4s^0$). The cubic crystal field at the Cu site splits the partially filled $3d$ levels into the lower energy t_{2g} ($|xy\rangle, |xz\rangle, |yz\rangle$), and the higher energy e_g ($|x^2-y^2\rangle, |3z^2-r^2\rangle$) manifold; the electronic configuration is $t_{2g}^6 e_g^3$. The co-operative Jahn-Teller distortion and the tetragonal compression further reduce the site symmetry of Cu, and the e_g doublet splits into $|3l^2-1\rangle$ and $|s^2-z^2\rangle$. Because long (l) and short (s) CuF bond alternate between $\mathbf{x}$ and $\mathbf{y}$ along all cubic axes, the highest energy d orbitals, $|s^2-z^2\rangle$, form the pattern shown in Fig. 2. The LDA band structure of $KCuF_3$ is shown in Fig. 3. We can identify the bands from their main character as F p-like (filled), Cu t_{2g}-like (filled), Cu e_g-like (occupied by 3 electrons), Cu s- and K s-like (empty). The Fermi level is located in the middle of the e_g-like bands.

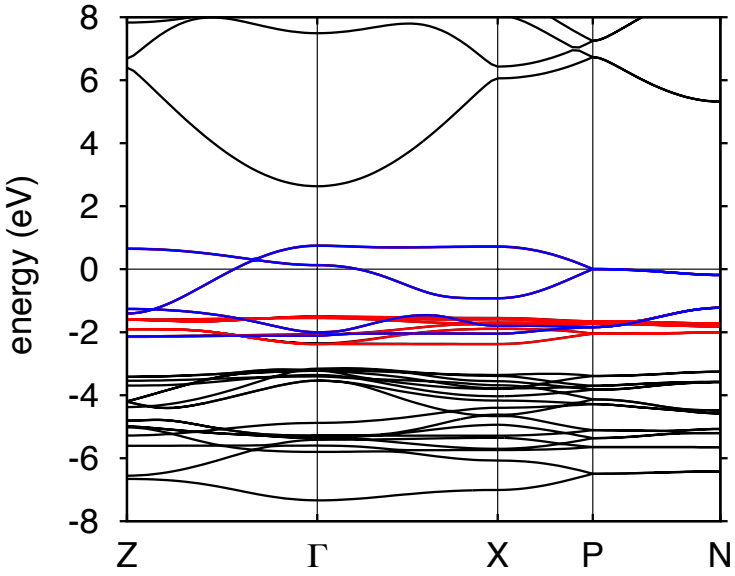

Fig. 3: *LDA band structure of $KCuF_3$. Blue: Cu e_g-like bands. Red: Cu t_{2g}-like bands. Black: filled F p-like bands and empty bands.*

Thus LDA predicts that $KCuF_3$ is a metal, although it actually is an insulator (paramagnetic down to $T_N = 40$ K). A similar problem occurs in many other transition-metal compounds with partially filled d shells: manganites, vanadates, titanates. This discrepancy cannot be solved by simple improvements of the LDA functional. Coulomb repulsion effects beyond mean field are essential to understand the origin of the insulating state in these materials. Other systems for which similar considerations apply are heavy fermions and Kondo systems (f electrons) or organics (molecular crystals).

2 Low-energy models

Lacking a working *ab-initio* theory, strongly-correlated systems have been studied for a long time through low-energy model Hamiltonians. Within this approach only the states and interactions believed to be most important to describe a given phenomenon are considered. Models can be justified on the ground that at low energy, high-energy degrees of freedom can be, in principle, projected out (*downfolded*), in the spirit of Wilson renormalization group. Their main effect is assumed to be included implicitly in the low-energy model through a renormalization of parameters. In LDA strongly-correlated transition-metal compounds usually have narrow d bands close to the Fermi level (see Fig. 3) and thus the d bands, or a subgroup of those (e_g-bands for $KCuF_3$) are believed to be the essential degrees of freedom. The minimal model to describe a system with a narrow band at the Fermi level is the Hubbard model

$$\hat{H} = -t \sum_{\sigma \langle ii' \rangle} c^\dagger_{i\sigma} c_{i'\sigma} + U \sum_i \hat{n}_{i\uparrow} \hat{n}_{i\downarrow} = \hat{H}_0 + \hat{U}, \tag{7}$$

where $c^\dagger_{i\sigma}$ ($c_{i\sigma}$) creates (destroys) an electron with spin σ at site i, $\hat{n}_{i\sigma} = c^\dagger_{i\sigma} c_{i\sigma}$ gives the i-site occupancy per spin, t is the hopping integral between first neighbors, and U the on-site Coulomb repulsion.
In the non-interacting limit ($U = 0$), the Hamiltonian (7) can be written in diagonal form

$$\hat{H}_0 = \sum_{\mathbf{k}\sigma} \varepsilon_{\mathbf{k}} c^\dagger_{\mathbf{k}\sigma} c_{\mathbf{k}\sigma} = \sum_{\mathbf{k}\sigma} \varepsilon_{\mathbf{k}} \hat{n}_{\mathbf{k}\sigma}.$$

The band energy is given by $\varepsilon_{\mathbf{k}} = -t\,\frac{1}{N}\sum_{\langle ii'\rangle} e^{i\mathbf{k}\cdot(\mathbf{R}_i - \mathbf{R}_{i'})}$, where $\mathbf{R}_i$ are lattice vectors, and N is the number of sites; the operator $c^\dagger_{\mathbf{k}\sigma}$ is the Fourier transform of $c^\dagger_{i\sigma}$, i.e., $c^\dagger_{\mathbf{k}\sigma} = \frac{1}{\sqrt{N}}\sum_i e^{i\mathbf{k}\cdot\mathbf{R}_i} c^\dagger_{i\sigma}$, and $\hat{n}_{\mathbf{k}\sigma} = c^\dagger_{\mathbf{k}\sigma} c_{\mathbf{k}\sigma}$. At half-filling ($N_e = N$), the ground state is paramagnetic and metallic.
In the atomic limit ($t = 0$), the model (7) describes instead an insulating collection of independent atoms with disordered magnetic moments.
Thus the Hubbard model captures the essence of the paramagnetic metal to paramagnetic insulator (Mott) transition, and can qualitatively explain why systems like $KCuF_3$ are paramagnetic insulators in a large temperature range. Furthermore, it explains the fact that $KCuF_3$ and most strongly-correlated transition-metal compounds have an antiferromagnetic ground state. For small t/U, by downfolding doubly occupied states, the Hubbard model (7) can be mapped onto a spin 1/2-antiferromagnetic Heisenberg model

$$\hat{H} \to J_{\rm AFM} \frac{1}{2} \sum_{\langle ii'\rangle} \left[\mathbf{S}_i \cdot \mathbf{S}_{i'} - \frac{1}{4} \hat{n}_i \hat{n}_{i'} \right],$$

with coupling $J_{\rm AFM} = 4t^2/U$. Thus at low temperature, when charge fluctuations play a minor role, a transition to an antiferromagnetic state can take place. In strongly-correlated transition-metal compounds, where the hopping t between correlated d states is mediated by the p orbitals of the atom between two transition metals (e.g., F p states in $KCuF_3$, Fig. 2), this many-body exchange mechanism is called *super-exchange*. Because the Hubbard model can be solved exactly only in special cases (e.g., in one dimension), it was for a long time impossible to understand the nature of the Mott transition within this model. Understanding real materials appeared even less likely. Progress came with the development of the dynamical mean-field theory (DMFT) [5]. In DMFT, the Hubbard model, which describes a lattice of correlated sites, is mapped onto an effective Anderson model, which describes a correlated *impurity*

$$\hat{H}_{\rm eff} = \sum_{\mathbf{k}\sigma} \varepsilon_{\mathbf{k}} \hat{n}_{\mathbf{k}\sigma} + \varepsilon_d \sum_\sigma \hat{n}_{d\sigma} + U \hat{n}_{d\uparrow} \hat{n}_{d\downarrow} + \sum_{\mathbf{k}\sigma} (V_{\mathbf{k}d}\; c^\dagger_{\mathbf{k}\sigma} d_\sigma + \overline{V}_{\mathbf{k}d}\; d^\dagger_\sigma c_{\mathbf{k}\sigma}).$$

Here $d^\dagger_\sigma$ (d_σ) creates (destroys) an electron at the impurity site, and $\hat{n}_{d\sigma} = d^\dagger_\sigma d_\sigma$ counts the number of electrons on the impurity; $c^\dagger_{\mathbf{k}\sigma}$ ($c_{\mathbf{k}\sigma}$) creates (destroys) a *bath* electron with energy $\varepsilon_{\mathbf{k}}$, and $V_{\mathbf{k}d}$ is the hybridization between bath and impurity. This auxiliary quantum-impurity model is solved self-consistently. The solution is found when the interacting Green function $G(\omega)$ of the auxiliary model equals the local Green function $G_{ii}(\omega)$ of the Hubbard model (7)

$$G(\omega) = G_{ii}(\omega) = \frac{1}{N_{\mathbf{k}}} \sum_{\mathbf{k}\in BZ} \frac{1}{\omega + \mu - \varepsilon_{\mathbf{k}} - \Sigma(\omega)} = \int d\varepsilon \frac{\rho(\varepsilon)}{\omega + \mu - \varepsilon - \Sigma(\omega)}. \qquad (8)$$

Here μ is the chemical potential, the sum is over $N_{\mathbf{k}}$ $\mathbf{k}$-points of the Brillouin Zone (BZ), $\Sigma(\omega)$ is the self-energy of the quantum impurity model and $\rho(\varepsilon)$ is the density of states. The self-energy $\Sigma(\omega)$ can be obtained from the Dyson equation of the impurity problem

$$\mathcal{G}^{-1}(\omega) = G^{-1}(\omega) + \Sigma(\omega), \tag{9}$$

where $\mathcal{G}(\omega)$ is the non-interacting Green function of the Anderson model (bath Green function). The main approximation in DMFT consists in neglecting spatial fluctuations in the lattice self-energy; this approximation becomes exact in the limit of infinite coordination number [5]. The Anderson model is a full many-body Hamiltonian, known since long in the framework of the Kondo effect [6], but, in contrast to the original Hubbard model, it describes only a single correlated site. It can be solved numerically with different approaches (*quantum-impurity solvers*): the numerical renormalization group [6], various flavors of quantum Monte Carlo (QMC) [7,8], Lanczos [9], or other methods [6,10]. Some of the most important solvers are presented in the Lectures of Erik Koch, Nils Blümer, and Philipp Werner. If we use QMC, we have to work in imaginary time/frequencies, and replace the frequency ω in (8, 9) with $i\omega_n$, where ω_n are Fermionic Matsubara frequencies, $\omega_n = (2n+1)\pi k_B T$, and T is the temperature.

The DMFT approach is discussed in detail in the Lecture of Marcus Kollar. We recall here some important conclusions obtained by studying the half-filled Bethe lattice, described for $U = 0$ by a semi-elliptical density of states [10]. In the Fermi-liquid regime (metallic phase, low temperature, $\omega \sim \mu = 0$), the self-energy can be expanded as

$$\Sigma(\omega + i0^+) \;\sim\; \frac{U}{2} + (1 - 1/Z)\omega - i\Delta\omega^2 + \dots .$$

The effective mass of quasi-particles is $m^* = m/Z$ and their life-time $\propto 1/\Delta$; Z is the quasi-particle weight. In the Mott insulating regime, the self-energy has instead the following low-frequency behavior

$$\Sigma(\omega + i0^+) \;\sim\; \frac{U}{2} + \Gamma/\omega - i\pi\Gamma\delta(\omega) + \dots ,$$

where Γ can be viewed as an order parameter. Thus the real part of the self-energy diverges at $\omega \sim 0$; the strong ω dependence of $\Sigma(\omega)$ is essential to obtain the Mott metal-insulator transition in the one-band Hubbard model.

The model Hamiltonian approach has proven effective in gaining insight into the behavior of strongly-correlated systems. However, the actual derivation of low-energy models by down-folding the full many-body problem, although formally possible, is in practice unfeasible and would in general lead to complex interactions beyond the Hubbard model [11]. The insight is thus gained at the price of neglecting all interactions that are thought not to have a direct influence on the specific phenomenon, and then relating the few free parameters (here t and U) to experimental data. It is clear that simple models such as the Hubbard model (7), although grasping an essential aspect of Mott physics, are hardly sufficient to describe the complexity of real materials such as $KCuF_3$. Thus they have been extended to include many orbitals (e.g., the full d shell), crystal-field splittings (which divides the d shell, e.g., into 3-fold degenerate t_{2g}

and 2-fold degenerate e_g states), multiplets (whose description requires taking into account the full Coulomb interaction tensor and the spin-orbit interaction), lattice distortions (which, in the case of $KCuF_3$, split the e_g and the t_{2g} manifold and change the hopping integrals), filled (e.g., F p in $KCuF_3$) or excited (Cu s, K s, ...) states, and Coulomb repulsion between neighbors. As we will see later in some examples, these *details do matter* when we want to understand real materials; neglecting them easily leads to wrong conclusions. Some of the parameters of such extended Hubbard models can indeed be obtained by fitting to experiments, but with the increasing number of free parameters it becomes impossible to put any theory to a real test.

3 Many-body models from DFT

3.1 Towards ab-initio Hamiltonians

The dream of calculating the parameters of model Hamiltonians *ab-initio* exists since long. We know from the successes of LDA that the Kohn-Sham orbitals obtained within the local-density approximation carry the essential information about the structure and chemistry of a given material. It appears therefore natural to build material-specific many-body models starting from the LDA. This can be achieved by constructing *ab-initio* a basis of localized LDA Wannier functions

$$\psi_{in\sigma}(\mathbf{r}) = \frac{1}{\sqrt{N}} \sum_{\mathbf{k}} e^{-i\mathbf{R}_i\cdot\mathbf{k}}\, \psi_{n\mathbf{k}\sigma}(\mathbf{r}),$$

and the corresponding many-body Hamiltonian, which is the sum of an LDA term $\hat{H}^{\rm LDA}$, a Coulomb term $\hat{U}$, and a double-counting correction $\hat{H}_{\rm DC}$

$$\hat{H}_e = \hat{H}^{\rm LDA} + \hat{U} - \hat{H}_{\rm DC}. \tag{10}$$

The LDA part of the Hamiltonian is given by

$$\hat{H}^{\rm LDA} = -\sum_{\sigma} \sum_{in,i'n'} t^{i,i'}_{n,n'} c^{\dagger}_{in\sigma} c_{i'n'\sigma}, \tag{11}$$

where $c^{\dagger}_{in\sigma}$ ($c_{in\sigma}$) creates (destroys) an electron with spin σ in orbital n at site i, and

$$t^{i,i'}_{n,n'} = -\int d\mathbf{r}\, \overline{\psi}_{in\sigma}(\mathbf{r})[-\frac{1}{2}\nabla^2 + v_{\rm R}(r)]\psi_{i'n'\sigma}(\mathbf{r}). \tag{12}$$

The on-site ($i = i'$) terms yield the crystal-field matrix while the $i \neq i'$ contributions are the hopping integrals. The Coulomb interaction $\hat{U}$ is given by

$$\hat{U} = \frac{1}{2} \sum_{ii'jj'} \sum_{\sigma\sigma'} \sum_{nn'pp'} U^{iji'j'}_{np\, n'p'} c^{\dagger}_{in\sigma} c^{\dagger}_{jp\sigma'} c_{j'p'\sigma'} c_{i'n'\sigma},$$

with

$$\begin{aligned} U^{iji'j'}_{np\, n'p'} &= \langle in\sigma\ jp\sigma'|\hat{U}|i'n'\sigma\ j'p'\sigma'\rangle \qquad (13)\\ &= \int d\mathbf{r}_1 \int d\mathbf{r}_2\, \overline{\psi}_{in\sigma}(\mathbf{r}_1)\overline{\psi}_{jp\sigma'}(\mathbf{r}_2)\frac{1}{|\mathbf{r}_1-\mathbf{r}_2|}\psi_{j'p'\sigma'}(\mathbf{r}_2)\psi_{i'n'\sigma}(\mathbf{r}_1). \end{aligned}$$

To avoid double counting, the correction $\hat{H}_{\rm DC}$ should cancel the electron-electron interaction contained in $\hat{H}^{\rm LDA}$, which in (10) is explicitly described by $\hat{U}$. However, it is more meaningful to take advantage of the LDA, and subtract from $\hat{U}$ the long-range Hartree and the mean-field exchange-correlation interaction, described by the LDA; from the successes of the LDA we expect that they are well accounted for. Thus the difference $\hat{U} - \hat{H}_{\rm DC}$ is a short-range many-body correction to the LDA.

The Hamiltonian (10) still describes the complete many-body problem, finding the solution of which remains an impossible task. To make progress, we separate the electrons in two types, the *correlated* or heavy electrons and the *uncorrelated* or light electrons. For the correlated electrons LDA fails qualitatively and $\hat{U} - \hat{H}_{\rm DC}$ has to be taken into account explicitly; we can assume that $\hat{U} - \hat{H}_{\rm DC}$ is local (on-site) or almost local (between near neighbors). For the uncorrelated electrons the LDA is overall a good approximation, and we do not consider any correction $\hat{U} - \hat{H}_{\rm DC}$. By truncating $\hat{U} - \hat{H}_{\rm DC}$ to the correlated sector we implicitly assume that the effect of light electrons is a mere renormalization or *screening* of Coulomb parameters in the correlated sector. This implies that the Coulomb couplings cannot be calculated directly from (13). The calculation of screened Coulomb integrals remains to date a major challenge, and effects beyond Coulomb parameter renormalization are usually neglected. Since correlated electrons partially retain their atomic character, in the rest of this Lecture we will label them with the quantum numbers $lm\sigma$, as in the atomic limit. To first approximation we can assume that $\hat{U} - \hat{H}_{\rm DC}$ is local and that correlated electrons belong to a single shell (e.g., d electrons, $l = 2$). Thus we can write the Hamiltonian as the generalized Hubbard model

$$\hat{H}_e = \hat{H}^{\rm LDA} + \hat{U}^l - \hat{H}^l_{\rm DC}, \tag{14}$$

where the *screened* Coulomb interaction is

$$\hat{U}^l = \frac{1}{2} \sum_i \sum_{\sigma\sigma'} \sum_{m_\alpha m'_\alpha} \sum_{m_\beta m'_\beta} U_{m_\alpha m_\beta m'_\alpha m'_\beta} c^\dagger_{im_\alpha\sigma} c^\dagger_{im_\beta\sigma'} c_{im'_\beta\sigma'} c_{im'_\alpha\sigma}, \tag{15}$$

and $\hat{H}^l_{\rm DC}$ is, in principle, the mean-field value of $\hat{U}^l$. More generally, we can include in the Hamiltonian (14) the Coulomb interaction between first neighbors, different shells, etc. Although (14) is simpler than the original model (10), it still describes a full many-body problem; however, as we will see later, such a problem can be solved numerically within the dynamical mean-field approximation.

At the heart of (14) is the assumption that the $\hat{U}^l - \hat{H}^l_{\rm DC}$ is local, or almost local; thus it is essential to use a localized basis in the correlated sector, a basis in which the separation of heavy and light electrons makes actually sense. Localized Wannier functions can be constructed in different ways. Successful methods are the *ab-initio* downfolding procedure based on the NMTO approach [12] and the maximally-localized Wannier functions algorithm of Marzari and Vanderbilt [13]; a lighter alternative to localized Wannier functions are projected local orbitals [14]. The latter two methods are presented in the Lecture of Jan Kuneš.

3.2 Coulomb interaction tensor

The screened Coulomb interaction, central to building the Hamiltonian (14), has the same form as the bare Coulomb interaction tensor. To identify the different terms in $\hat{U}^l$, it is useful to derive the bare Coulomb integrals for atomic orbitals $\psi_{nlm}(\mathbf{r}) = R_{nl}(r)Y^l_m(\theta,\phi)$ (see Appendix B). The generalization to Wannier orbitals is straightforward. First, we write the electronic positions in spherical coordinates, $\mathbf{r}_i = r_i(\sin\theta_i\cos\phi_i, \sin\theta_i\sin\phi_i, \cos\theta_i)$, and express the Coulomb interaction as

$$\frac{1}{|\mathbf{r}_1-\mathbf{r}_2|} = \sum_{k=0}^{\infty} \frac{r_<^k}{r_>^{k+1}} \frac{4\pi}{2k+1} \sum_{q=-k}^{k} Y^k_q(\theta_2,\phi_2)\overline{Y}^k_q(\theta_1,\phi_1), \tag{16}$$

where $r_<$ ($r_>$) is the smaller (larger) of r_1 and r_2. By inserting (16) into (13) we obtain

$$U_{m_\alpha m_\beta m'_\alpha m'_\beta} = \sum_{k=0}^{2l} a_k(m_\alpha m'_\alpha, m_\beta m'_\beta) F_k,$$

where a_k are angular integrals

$$a_k(m_\alpha m'_\alpha, m_\beta m'_\beta) = \frac{4\pi}{2k+1} \sum_{q=-k}^{k} \langle lm_\alpha|Y^k_q|lm'_\alpha\rangle \langle lm_\beta|\overline{Y}^k_q|lm'_\beta\rangle,$$

and F_k radial Slater integrals

$$F_k = \int dr_1\, r_1^2 \int dr_2\, r_2^2\, R^2_{nl}(r_1) \frac{r_<^k}{r_>^{k+1}} R^2_{nl}(r_2).$$

The most important Coulomb integrals are the two-index terms: the direct ($U_{mm'mm'}$) and exchange ($U_{mm'm'm}$, with $m \neq m'$) integrals, which can be expressed as

$$\begin{aligned} U_{mm'mm'} = U_{m,m'} &= \sum_{k=0}^{2l} a_k(mm, m'm') F_k, \\ U_{mm'm'm} = J_{m,m'} &= \sum_{k=0}^{2l} a_k(mm', m'm) F_k. \end{aligned}$$

It can be shown that $U_{m,m'}$ and $J_{m,m'}$ are positive, and that $U_{m,m'} \geq J_{m,m'}$. If we neglect all terms but the direct and the exchange Coulomb interaction, only density-density terms ($\propto \hat{n}_{im\sigma}\hat{n}_{im'\sigma'}$, with $\hat{n}_{im\sigma} = c^\dagger_{im\sigma}c_{im\sigma}$) remain, and the Coulomb interaction takes a simpler form

$$\hat{U}^l \sim \frac{1}{2}\sum_{i\sigma}\sum_{mm'} U_{m,m'}\hat{n}_{im\sigma}\hat{n}_{im'\text{-}\sigma} + \frac{1}{2}\sum_{i\sigma}\sum_{m\neq m'} (U_{m,m'} - J_{m,m'})\hat{n}_{im\sigma}\hat{n}_{im'\sigma}. \tag{17}$$

The contributions neglected in (17), spin-flip exchange terms ($\propto J_{m,m'}$) and off-diagonal contributions (terms with more than two different orbital indices), are important to get the correct multiplet structure. They are often neglected in DMFT calculations based on QMC solvers because they can generate a strong sign problem.

In electronic-structure calculations real harmonics (Appendix B) rather than spherical harmonics are normally used; therefore here we will give the Coulomb integrals for d electrons in the basis of real harmonics. It is useful to introduce first average Coulomb parameters

$$U_{avg} = \frac{1}{(2l+1)^2}\sum_{m,m'} U_{m,m'} = F_0,$$

$$U_{avg} - J_{avg} = \frac{1}{2l(2l+1)}\sum_{m,m'}(U_{m,m'} - J_{m,m'}).$$

For d-electrons, only F_0, F_2 and F_4 contribute to the Coulomb integrals, and we can show that $J_{\rm avg} = (F_2 + F_4)/14$. For hydrogen-like $3d$ orbitals, $F_4/F_2 = 15/23$, while for realistic $3d$ orbitals this ratio is slightly smaller. A typical value is $F_4/F_2 \sim 0.625 = 5/8$.
The parameters $U^l_{m,m'}$ may be written as

$U^l_{m,m'}$	$\|xy\rangle$	$\|yz\rangle$	$\|3z^2-r^2\rangle$	$\|xz\rangle$	$\|x^2-y^2\rangle$
$\|xy\rangle$	U_0	U_0-2J_1	U_0-2J_2	U_0-2J_1	U_0-2J_3
$\|yz\rangle$	U_0-2J_1	U_0	U_0-2J_4	U_0-2J_1	U_0-2J_1
$\|3z^2-r^2\rangle$	U_0-2J_2	U_0-2J_4	U_0	U_0-2J_4	U_0-2J_2
$\|xz\rangle$	U_0-2J_1	U_0-2J_1	U_0-2J_4	U_0	U_0-2J_1
$\|x^2-y^2\rangle$	U_0-2J_3	U_0-2J_1	U_0-2J_2	U_0-2J_1	U_0

where

$$\begin{aligned}
U_0 &= U_{\rm avg} + \frac{8}{7}J_{\rm avg} = U_{\rm avg} + \frac{8}{5}\mathcal{J}_{\rm avg}\\
J_1 &= \frac{3}{49}F_2 + \frac{20}{9}\frac{1}{49}F_4\\
J_2 &= -2\mathcal{J}_{\rm avg} + 3J_1\\
J_3 &= 6\mathcal{J}_{\rm avg} - 5J_1\\
J_4 &= 4\mathcal{J}_{\rm avg} - 3J_1.
\end{aligned}$$

The parameter $\mathcal{J}_{avg}$ is the actual average of the exchange terms in the basis of real harmonics

$$\mathcal{J}_{avg} = \frac{1}{2l(2l+1)}\sum_{m\neq m'} J_{m,m'} = \frac{5}{7}J_{\rm avg}.$$

For atomic d states, $U_{\rm avg}$ is very large ($15-20$ eV), but screening effects reduce it drastically. The calculation of screening effects is very difficult because it is basically equivalent to finding the solution of the full many-body problem. Approximate schemes are the constrained LDA (cLDA) approach [16] and the constrained RPA (cRPA) method [17]. In cLDA, the screened U is obtained from the second derivative of the total energy as a function of the density; to avoid electron transfer between correlated and uncorrelated sectors, the hopping integrals between heavy and light electrons are cut. In cRPA the polarization (and thus the screened Coulomb interaction) is obtained in the random-phase approximation by downfolding the uncorrelated sector, assuming that the latter is well described by mean field. These approaches are discussed in the Lecture of Ferdi Aryasetiawan.

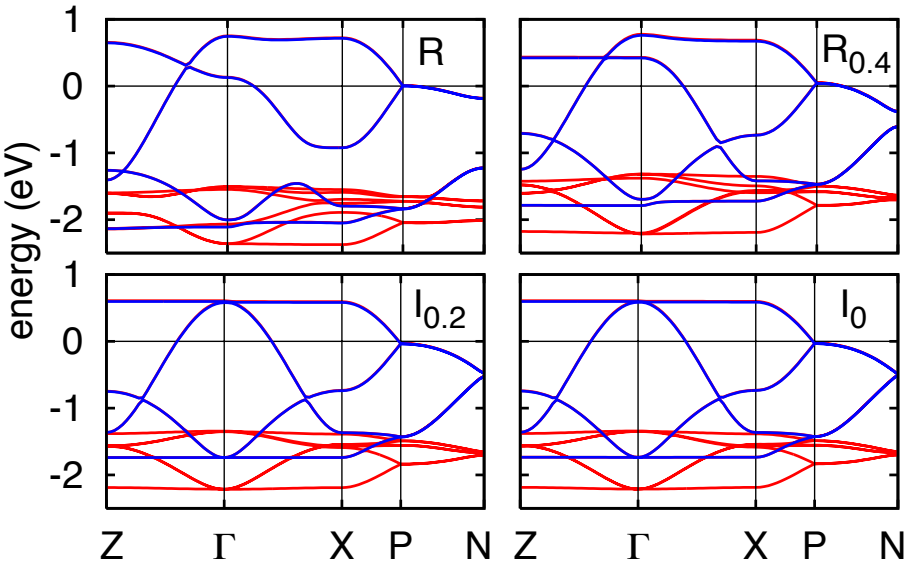

Fig. 4: *LDA e_g (blue) and t_{2g}(red) band structure of $KCuF_3$ for the experimental structure (R) and ideal structures with progressively reduced distortions (see Fig. 2). I_0: simple cubic. The unit cell contains 2 formula units. From Ref. [4].*

3.3 Minimal material-specific models

To understand a given system it is convenient to make the correlated electron sector as small as possible, while still retaining the crucial degrees of freedom. To this end we have to construct *minimal model Hamiltonians*, which are still material specific but have as few degrees of freedom and parameters as possible. Here we will see how this can be achieved through massive downfolding of the LDA Hamiltonian. As example we consider the case of $KCuF_3$ in tight-binding theory. For simplicity, we neglect the tetragonal and Jahn-Teller distortions. In the cubic structure, the primitive cell contains one formula unit (a single K cube in Fig. 2). The cubic axes are $\mathbf{x}$, $\mathbf{y}$, $\mathbf{z}$, and the lattice constant a. A Cu atom at site $\mathbf{R}_i$ is surrounded by two apical F atoms, F_1 at $\mathbf{R}_i + \frac{1}{2}\mathbf{z}$ and F_2 at $\mathbf{R}_i - \frac{1}{2}\mathbf{z}$, and four planar F atoms, F_3 and F_4 at $\mathbf{R}_i \pm \frac{1}{2}\mathbf{x}$ and F_5 and F_6 at $\mathbf{R}_i \pm \frac{1}{2}\mathbf{y}$. In Fig. 4 one can see the effects of the cubic approximation on the e_g bands: the crystal-field splitting of e_g states is zero, the band width slightly reduced, gaps disappear, and the dispersion relations is sizably modified (e.g., along ΓZ). We take as Wannier basis the atomic $3d$ e_g orbitals for Cu and the $2p$ orbitals for F; we neglect the overlap integrals and all other states. The main contribution to the hopping integrals (12) are the Slater-Koster two-center matrix elements (Appendix B). In the case described, the only relevant Slater-Koster parameter is $V_{pd\sigma}$. The $|3z^2 - r^2\rangle_i$ and $|x^2 - y^2\rangle_i$ states of the Cu at $\mathbf{R}_i$ are coupled via $V_{pd\sigma}$ to $|z\rangle_i$, the p_z orbitals of F_1 and F_2, to $|x\rangle_i$, the p_x orbitals of F_3 and F_4 and to $|y\rangle_i$, the p_y orbitals of F_5 and F_6. From the basis $|\alpha\rangle_i$ (where $\alpha = x, y, z, 3z^2 - r^2, x^2 - y^2$), we construct the Bloch states $|\mathbf{k}\alpha\rangle = \frac{1}{\sqrt{N}} \sum_i e^{i\mathbf{k}\cdot\mathbf{R}_i} |\alpha\rangle_i$, and obtain the tight-binding Hamiltonian

$H^{\rm TB}$	$\vert\mathbf{k}\ z\rangle$	$\vert\mathbf{k}\ x\rangle$	$\vert\mathbf{k}\ y\rangle$	$\vert\mathbf{k}\ 3z^2-r^2\rangle$	$\vert\mathbf{k}\ x^2-y^2\rangle$
$\vert\mathbf{k}\ z\rangle$	ε_p	0	0	$-2V_{pd\sigma}s_z$	0
$\vert\mathbf{k}\ x\rangle$	0	ε_p	0	$V_{pd\sigma}s_x$	$-\sqrt{3}V_{pd\sigma}s_x$
$\vert\mathbf{k}\ y\rangle$	0	0	ε_p	$V_{pd\sigma}s_y$	$\sqrt{3}V_{pd\sigma}s_y$
$\vert\mathbf{k}\ 3z^2-r^2\rangle$	$-2V_{pd\sigma}\overline{s}_z$	$V_{pd\sigma}\overline{s}_x$	$V_{pd\sigma}\overline{s}_y$	ε_d	0
$\vert\mathbf{k}\ x^2-y^2\rangle$	0	$-\sqrt{3}V_{pd\sigma}\overline{s}_x$	$\sqrt{3}V_{pd\sigma}\overline{s}_y$	0	ε_d

(18)

where $s_\alpha = ie^{-ik_\alpha a/2}\sin k_\alpha a/2$, $\alpha = x, y, z$, $\varepsilon_p < \varepsilon_d = \varepsilon_p + \Delta_{pd}$, and $V_{pd\sigma} < 0$. If $|V_{pd\sigma}|/\Delta_{pd}$ is small, the occupied bands are F p-like, while the partially filled bands Cu e_g-like. We now calculate the bands along high-symmetry lines.[1] Along ΓZ, the eigenvalues ε_i ($\varepsilon_i \le \varepsilon_{i+1}$) of $H^{\rm TB}$ are

$$\begin{aligned}
\varepsilon_2 &= \varepsilon_p \\
\varepsilon_3 &= \varepsilon_p \\
\varepsilon_4 &= \varepsilon_d \\
\varepsilon_{1,5} &= \varepsilon_p + \tfrac{1}{2}\Delta_{pd} \pm \tfrac{1}{2}\sqrt{\Delta_{pd}^2 + 16V_{pd\sigma}^2|s_z|^2}
\end{aligned}$$

where ε_1 is bonding and F z-like, while ε_5 anti-bonding and $3z^2-r^2$-like. Along ΓX, we have instead the dispersion relations

$$\begin{aligned}
\varepsilon_2 &= \varepsilon_p \\
\varepsilon_3 &= \varepsilon_p \\
\varepsilon_4 &= \varepsilon_d \\
\varepsilon_{1,5} &= \varepsilon_p + \tfrac{1}{2}\Delta_{pd} \pm \tfrac{1}{2}\sqrt{\Delta_{pd}^2 + 16V_{pd\sigma}^2|s_x|^2}
\end{aligned}$$

where ε_1 is bonding and F x-like, while ε_5 anti-bonding and x^2-y^2-like.
To obtain the e_g-like bands, instead of diagonalizing $H^{\rm TB}$ as we have done above, we can also use the downfolding procedure, which, for independent electrons, can be done exactly. We divide the orbitals in passive (F p) and active (Cu d), and write the eigenvalues equation as

$$\begin{bmatrix} H_{pp} & H_{pd} \\ H_{dp} & H_{dd} \end{bmatrix} \begin{bmatrix} \vert\mathbf{k}\ p\rangle \\ \vert\mathbf{k}\ d\rangle \end{bmatrix} = \varepsilon \begin{bmatrix} I_{pp} & 0 \\ 0 & I_{dd} \end{bmatrix} \begin{bmatrix} \vert\mathbf{k}\ p\rangle \\ \vert\mathbf{k}\ d\rangle \end{bmatrix},$$

where H_{pp} (I_{pp}) is the Hamiltonian (identity matrix) in the p-electron space (3×3), and H_{dd} (I_{dd}) the Hamiltonian (identity matrix) in the d-electron space (2×2). By downfolding to the d sector we obtain the energy-dependent operator H_{dd}^{ε}, which acts in the d space

$$H_{dd}^{\varepsilon} = H_{dd} - H_{dp}(H_{pp} - \varepsilon I_{pp})^{-1}H_{pd},$$

and a correspondingly transformed and energy-dependent basis set for the active space, $\vert\mathbf{k}\ d\rangle_\varepsilon$. The operator H_{dd}^{ε} has the same eigenvalues and eigenvectors as the original Hamiltonian. In the case of $KCuF_3$

H_{dd}^{ε}	$\vert\mathbf{k}\ 3z^2-r^2\rangle_\varepsilon$	$\vert\mathbf{k}\ x^2-y^2\rangle_\varepsilon$
$\vert\mathbf{k}\ 3z^2-r^2\rangle_\varepsilon$	$\varepsilon'_d - 2t_\varepsilon[\frac{1}{4}(\cos k_x a + \cos k_y a) - \cos k_z a]$	$2t_\varepsilon[\frac{\sqrt{3}}{4}(\cos k_x a - \cos k_y a)]$
$\vert\mathbf{k}\ x^2-y^2\rangle_\varepsilon$	$2t_\varepsilon[\frac{\sqrt{3}}{4}(\cos k_x a - \cos k_y a)]$	$\varepsilon'_d - 2t_\varepsilon[\frac{3}{4}(\cos k_x a + \cos k_y a)]$

(19)

[1] Special points: $\Gamma = (0,0,0)$, Z$= (0,0,\pi/a)$, X$= (\pi/a,0,0)$, M$= (\pi/a,\pi/a,0)$, R$= (\pi/a,\pi/a,\pi/a)$.

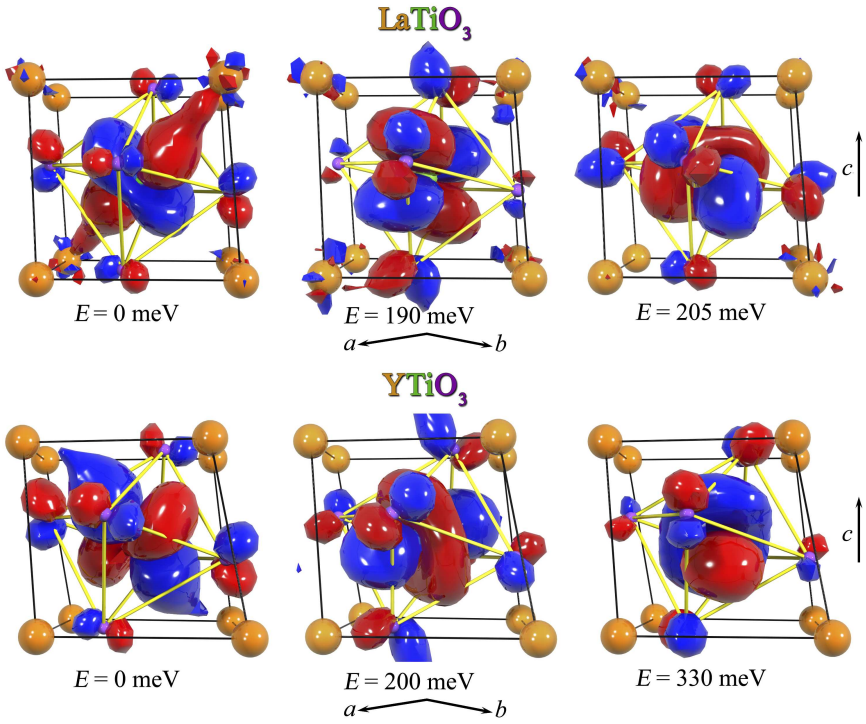

Fig. 5: *Crystal-field t_{2g} Wannier orbitals and corresponding crystal-field energies in the $3d^1$ perovskites $LaTiO_3$ and $YTiO_3$. La/Y: orange. Ti: red. O: violet. From Ref. [12].*

where $t_\varepsilon = V_{pd\sigma}^2/(\varepsilon - \varepsilon_p)$, $\varepsilon_d' = \varepsilon_d + 3t_\varepsilon$, and $|\mathbf{k}\ 3z^2 - r^2\rangle_\varepsilon$, $|\mathbf{k}\ x^2 - y^2\rangle_\varepsilon$ is the new basis set, which retains however the original ($3z^2 - r^2$ or $x^2 - y^2$) symmetry. The downfolding procedure has *renormalized* the parameters ε_d of the original model (18), but also introduced a new interaction: inter-orbital matrix elements. Furthermore, H_{dd}^ε and the Bloch basis are now energy dependent. Along ΓZ, the eigenvalues of (19) are given implicitly by the equations $\varepsilon = \varepsilon_d + 2t_\varepsilon - 2t_\varepsilon \cos k_z a$ and $\varepsilon = \varepsilon_d$; in second-order perturbation theory $t_\varepsilon \sim t_{\varepsilon_d} = V_{pd\sigma}^2/\Delta_{pd}$, $\varepsilon \sim \varepsilon_d + 2t_{\varepsilon_d} - 2t_{\varepsilon_d} \cos k_z a$, $\varepsilon = \varepsilon_d$. From Hamiltonian (19) it is easy to see that the e_g bands are 2-fold degenerate along ΓR, to find the dispersion along ΓM and RM, and obtain the e_g-like bands in Fig. 4. From the Bloch states $|\mathbf{k}\ 3z^2 - r^2\rangle_\varepsilon$ and $|\mathbf{k}\ x^2 - y^2\rangle_\varepsilon$, we may build new Wannier functions. They have $3z^2 - r^2$ or $x^2 - y^2$ symmetry as the original ones but also span, to arbitrary accuracy, the e_g bands. These new Wannier functions are longer range than the original atomic orbitals, since they have p tails on the downfolded neighboring F sites.

The same downfolding procedure can be performed *ab-initio*, e.g., using DFT approaches based on atomic-like orbitals, such as the NMTO method. It leads to ab-initio Wannier functions, which carry the information on the lattice structure and the chemistry [12]. The higher energy crystal-field orbital of $KCuF_3$ (experimental structure), calculated in this way, is shown in Fig. 2.

Another example of Wannier functions is shown in Fig. 5. $LaTiO_3$ and $YTiO_3$ have a perovskite structure as $KCuF_3$, but the O octahedra are tilted and rotated and the La/Y cages are strongly distorted. To obtain the t_{2g} crystal-field Wannier orbitals in Fig. 5 we downfold all other states but the t_{2g}. Although the Ti atoms form an almost cubic lattice, the t_{2g} Wannier functions reflect

the actual distorted structure, as do the corresponding hopping integrals; thus the t_{2g} orbitals are not degenerate, as they would be in a cubic lattice.
Once we have obtained the basis and the hopping integrals, we construct $H = \hat{H}^{\rm LDA} + \hat{U}^l - \hat{H}^l_{\rm DC}$. For the e_g doublet we can express $\hat{U}^l$ in a simpler form, because only two-index Coulomb terms are present; furthermore, $U_{m,m'} = U - 2J(1-\delta_{m,m'})$ and, for $m \neq m'$, $J_{m,m'} = J$, where $U = U_0$ and $J = J_2$. Thus the e_g Hubbard model has the form

$$\begin{aligned} H= & -\sum_{m,m',i,i',\sigma} t^{i,i'}_{mm'} c^\dagger_{im\sigma} c_{im'\sigma} + U \sum_{i\ m} \hat{n}_{im\uparrow}\hat{n}_{im\downarrow} \\ & + \frac{1}{2}\sum_{\substack{i\sigma\sigma' \\ m\neq m'}} (U - 2J - J\delta_{\sigma,\sigma'}) \hat{n}_{im\sigma}\hat{n}_{im'\sigma'} \\ & - J \sum_{i\ m\neq m'} \left[c^\dagger_{im\uparrow} c^\dagger_{im\downarrow} c_{im'\uparrow} c_{im'\downarrow} + c^\dagger_{im\uparrow} c_{im\downarrow} c^\dagger_{im'\downarrow} c_{im'\uparrow} \right] - \hat{H}^{e_g}_{\rm DC}, \end{aligned} \tag{20}$$

where $m, m' = 3z^2 - r^2, x^2 - y^2$. The last two terms describe the pair-hopping ($U_{mmm'm'} = J_{m,m'}$ for real harmonics, while for spherical harmonics $U_{mmm'm'} = 0$) and spin-flip processes. The Hamiltonian has the same form (however with $J = J_1$) for systems with partially filled t_{2g} bands, e.g., $LaTiO_3$ and $YTiO_3$.
Massive downfolding to few-band models (for $KCuF_3$ the e_g bands) necessarily leads to longer range Wannier functions. On the other hand, working with the full Hamiltonian has the drawback that the large number of parameters makes it difficult to gain insight in the problem, losing the advantage of model physics. Another advantage of massive downfolding to a given set of correlated states is that the double-counting correction becomes an energy shift. We can incorporate it into the chemical potential, which is obtained self-consistently from the number of correlated electrons, getting rid of an essentially unknown term.

4 Methods of solution

4.1 LDA+U

The first systematic attempt to construct and solve *ab-initio* many-body Hamiltonians was the LDA+*U* method [15]. In this approach the Coulomb interaction is treated in static mean-field theory (in the spirit of Hartree-Fock), and therefore true many-body effects are lost. However, the problems that we have to face in constructing the Hamiltonian (14) are the same, independently of how the Coulomb interaction is then treated. To we explain how LDA+*U* works, we assume that Hamiltonian (14) has the simplified form

$$\hat{H}^{\rm LDA} + \hat{U}^l - \hat{H}^l_{\rm DC} = \hat{H}^{\rm LDA} + \frac{1}{2}U \sum_{i} \sum_{m\sigma\neq m'\sigma'} \hat{n}_{im\sigma}\hat{n}_{im'\sigma'} - \frac{1}{2}U \sum_{i} \sum_{m\sigma\neq m'\sigma'} \langle \hat{n}_{im\sigma}\rangle \langle \hat{n}_{im'\sigma'}\rangle .$$

We treat the Coulomb interaction in static mean-field at the Hartree level,

$$\hat{n}_{im\sigma}\hat{n}_{im'\sigma'} \rightarrow \langle \hat{n}_{im\sigma}\rangle \hat{n}_{im'\sigma'} + \hat{n}_{im\sigma}\langle \hat{n}_{im'\sigma'}\rangle - \langle \hat{n}_{im\sigma}\rangle \langle \hat{n}_{im'\sigma'}\rangle ,$$

and approximate the mean-field energy $\frac{1}{2}U\sum_{m\sigma\neq m'\sigma'}\langle\hat{n}_{im\sigma}\rangle\langle\hat{n}_{im'\sigma'}\rangle$ by the Hartree energy $\frac{1}{2}UN^lN^l$, where $N^l=\sum_{m\sigma}\langle\hat{n}_{im\sigma}\rangle$ is the number of heavy electrons per site. The mean-field Hamiltonian is

$$H=\hat{H}^{\rm LDA}+\sum_{im\sigma}t^\sigma_m\hat{n}_{im\sigma},\quad\text{with}\quad t^\sigma_m=U(\frac{1}{2}-\langle\hat{n}_{im\sigma}\rangle).$$

The levels of the correlated electrons are shifted by $-U/2$ if occupied and by $U/2$ if empty, like in the atomic limit of the half-filled Hubbard model. A total energy functional which shifts the orbital energies in this way is

$$E_{\rm LDA+U}[n]=E_{\rm LDA}[n]+\sum_i\left[\frac{1}{2}U\sum_{m\sigma\neq m'\sigma'}\langle\hat{n}_{im\sigma}\rangle\langle\hat{n}_{im'\sigma'}\rangle-E_{\rm DC}\right],$$

where $E_{\rm DC}=\frac{1}{2}UN^l(N^l-1)$ and $E_{LDA}[n]$ is the total energy obtained using the spin-polarized version of the local-density approximation (LSDA) for the exchange-correlation functional. Indeed

$$\varepsilon^{\rm LDA+U}_{im\sigma}=\frac{\partial E_{\rm LDA+U}}{\partial\langle\hat{n}_{im\sigma}\rangle}=\varepsilon^{\rm LDA}_{im\sigma}+U(\frac{1}{2}-\langle\hat{n}_{im\sigma}\rangle).$$

More generally, if $\hat{U}^l$ has the form (15), the LDA+*U* functional is given by

$$\begin{aligned}E_{\rm LDA+U}[n] &= E_{\rm LDA}[n]+\frac{1}{2}\sum_{i\sigma}\sum_{mm'm''m'''}U_{mm''m'm'''}\langle\hat{n}^\sigma_{imm'}\rangle\langle\hat{n}^{-\sigma}_{im''m'''}\rangle\\ &+ \frac{1}{2}\sum_{i\sigma}\sum_{mm'm''m'''}\left[U_{mm''m'm'''}-U_{mm''m'''m'}\right]\langle\hat{n}^\sigma_{imm'}\rangle\langle\hat{n}^\sigma_{im''m'''}\rangle-E_{\rm DC},\end{aligned}$$

where $\langle\hat{n}^\sigma_{imm'}\rangle=\langle c^\dagger_{im\sigma}c_{im'\sigma}\rangle$ is the density matrix, and $\langle\hat{n}_{im\sigma}\rangle=\langle\hat{n}^\sigma_{imm}\rangle$. One of the most common recipe for the double-counting correction is

$$E_{\rm DC}=\frac{1}{2}U_{avg}N^l(N^l-1)-\frac{1}{2}J_{avg}\sum_\sigma N^l_\sigma(N^l_\sigma-1).\tag{21}$$

The corresponding one-electron LDA+*U* Hamiltonian is

$$\hat{H}=\hat{H}^{\rm LDA}+\sum_{imm'\sigma}t^\sigma_{mm'}c^\dagger_{im\sigma}c_{im'\sigma},\tag{22}$$

where[2]

$$\begin{aligned}t^\sigma_{mm'} &= \sum_{i\sigma}\sum_{m''m'''}U_{mm''m'm'''}\langle\hat{n}^{-\sigma}_{im''m'''}\rangle+\left[U_{mm''m'm'''}-U_{mm''m'''m'}\right]\langle\hat{n}^\sigma_{im''m'''}\rangle\\ &- \left[U_{avg}(N^l-\frac{1}{2})-J_{avg}(N^l_\sigma-\frac{1}{2})\right]\delta_{m,m'}.\end{aligned}$$

In LDA+*U*, differently than in static mean-field for a given Hamiltonian, $\hat{H}^{\rm LDA}$ is obtained self-consistently. The LDA+*U* correction in (22) modifies the occupations of the correlated sector

[2]The LDA+*U* correction to the parameters of the LDA Hamiltonian may be obtained from the derivative of $E_{\rm LSDA+U}[n]$ with respect to the density matrix.

with respect to LDA. If we assume that LDA describes uncorrelated electrons sufficiently well, the readjustments in the uncorrelated sector can be calculated by making the total charge density and the reference potential consistent within the LDA (*charge self-consistency*), however with the constraint given by (22). LDA+*U* calculations are usually not performed in a Wannier basis. They are typically based on the identification of an *atomic sphere*, a region of space in which correlated electrons are well described by atomic-like orbitals; the LDA+*U* correction is determined through projections onto such atomic orbitals. Thus LDA+*U* results are essentially dependent on the choice of the set of correlated electrons and this atomic sphere. However, if the correlated electrons are well localized, they retain indeed to a good extent their atomic character in a solid. Thus the arbitrariness of the choice is less crucial than could be expected. Calculations based on different electronic structure methods confirm this.

LDA+*U* describes successfully the magnetic ground-state of Mott insulators. This could appear surprising, because the LDA+*U* Hamiltonian (22) describes a non-interacting system, and therefore should in principle have the same defects of the LDA Hamiltonian. However, LDA+*U* opens a gap by making long-range order (magnetic, magnetic and orbital, ...). Indeed, in some cases we obtain a gap already in LSDA, although often such a gap is much smaller than the experimental one. As in LDA, the LDA+*U* eigenvalues are real, and quasi-particles have an infinite lifetime. In the Green function language, LDA+*U* yields a self-energy which is orbital, spin, and site dependent within the unit cell, but has no ω dependence and no imaginary part.

We present as an example the case of $KCuF_3$. Instead of the full LDA+*U* calculation, for simplicity we discuss the results for the e_g-band Hubbard model (20) and do not perform any charge self-consistency. We study the ideal cubic structure; the independent-electron part of the Hamiltonian is given to a good approximation by Eq. (19). We consider a unit cell with axes $\mathbf{a} = (-\mathbf{x} + \mathbf{y})$, $\mathbf{b} = (\mathbf{x} + \mathbf{y})$, $\mathbf{c} = 2\mathbf{z}$. This cell contains four octahedra. The four Cu atoms are located at $(0, 0, 0)$, $(a/2, a/2, 0)$, $(0, 0, a/2)$, $(a/2, a/2, a/2)$; we label them as $1_u, 2_u, 1_d, 2_d$. The difference between sites of type 1 and 2 in the experimental structure with the co-operative Jahn-Teller distortion is illustrated in Fig. 2; in the cubic structure they are identical. The metallic paramagnetic LDA band structure for this supercell is shown in Fig. 6. The insulating static mean-field bands are shown on the left. In the basis $|\alpha\sigma\rangle_i$, $|\beta\sigma\rangle_i$, with $\alpha = 3z^2 - r^2$, and $\beta = x^2 - y^2$, the LDA+*U* self-energy for a site i has the following form

$$\Sigma^{i\sigma} = \begin{bmatrix} \Sigma^{i\sigma}_{\alpha,\alpha} & \Sigma^{i\sigma}_{\alpha,\beta} \\ \Sigma^{i\sigma}_{\beta,\alpha} & \Sigma^{i\sigma}_{\beta,\beta} \end{bmatrix}.$$

Setting for simplicity $J = 0$ we find

$$\Sigma^{i\sigma} = U \begin{bmatrix} \frac{1}{2} - \langle \hat{n}^{\sigma}_{i\alpha\alpha} \rangle & -\langle \hat{n}^{\sigma}_{i\beta\alpha} \rangle \\ -\langle \hat{n}^{\sigma}_{i\alpha\beta} \rangle & \frac{1}{2} - \langle \hat{n}^{\sigma}_{i\beta\beta} \rangle \end{bmatrix},$$

where the density matrix has to be determined self-consistently. The static mean-field bands in the left panel of Fig. 6 correspond approximatively to a state with one hole in $|z^2 - y^2\uparrow\rangle = \frac{\sqrt{3}}{2}|\alpha\uparrow\rangle + \frac{1}{2}|\beta\uparrow\rangle$ at site 1_u, in $|z^2 - y^2\downarrow\rangle$ at site 1_d, in $|z^2 - x^2\uparrow\rangle$ at site 2_u, and in $|z^2 - x^2\downarrow\rangle$ at site 2_d. Correspondingly, the self-energy matrix may be written as

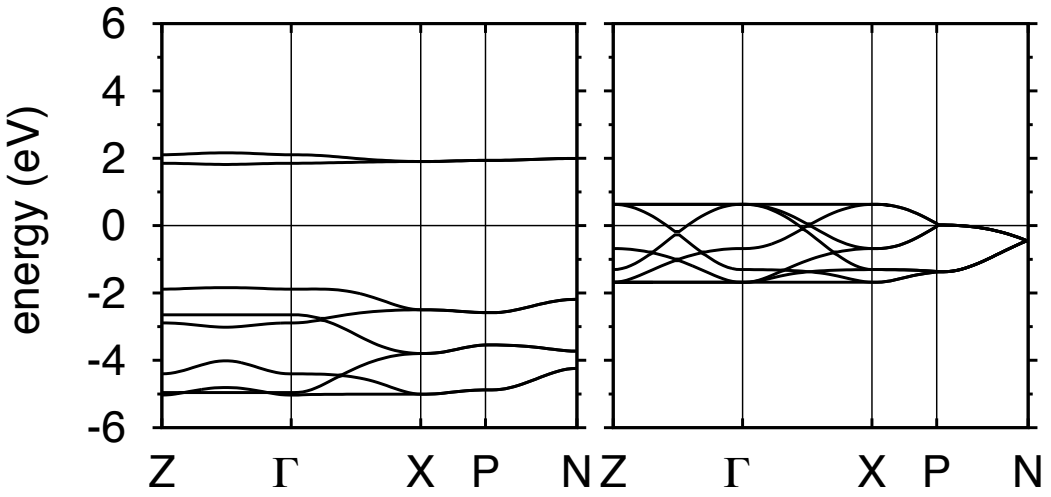

Fig. 6: *Right: LDA e_g band structure of cubic $KCuF_3$ calculated using the experimental magnetic unit cell with four formula units. Left: Static mean-field band structure, calculated for the experimental orbital and spin order. Parameters: $U = 7\ eV$ and $J = 0.9$ eV.*

Σ/U	$\|\alpha\sigma\rangle_{1_u}$	$\|\beta\sigma\rangle_{1_u}$	$\|\alpha\sigma\rangle_{2_u}$	$\|\beta\sigma\rangle_{2_u}$	$\|\alpha\sigma\rangle_{1_d}$	$\|\beta\sigma\rangle_{1_d}$	$\|\alpha\sigma\rangle_{2_d}$	$\|\beta\sigma\rangle_{2_d}$
$\|\alpha\sigma\rangle_{1_u}$	$\frac{-2\delta_{\sigma,\downarrow}-\delta_{\sigma,\uparrow}}{4}$	$\frac{\sqrt{3}\delta_{\sigma,\uparrow}}{4}$	0	0	0	0	0	0
$\|\beta\sigma\rangle_{1_u}$	$\frac{\sqrt{3}\delta_{\sigma,\uparrow}}{4}$	$\frac{-2\delta_{\sigma,\downarrow}+\delta_{\sigma,\uparrow}}{4}$	0	0	0	0	0	0
$\|\alpha\sigma\rangle_{2_u}$	0	0	$\frac{-2\delta_{\sigma,\downarrow}-\delta_{\sigma,\uparrow}}{4}$	$\frac{-\sqrt{3}\delta_{\sigma,\uparrow}}{4}$	0	0	0	0
$\|\beta\sigma\rangle_{2_u}$	0	0	$\frac{-\sqrt{3}\delta_{\sigma,\uparrow}}{4}$	$\frac{-2\delta_{\sigma,\downarrow}+\delta_{\sigma,\uparrow}}{4}$	0	0	0	0
$\|\alpha\sigma\rangle_{1_d}$	0	0	0	0	$\frac{-2\delta_{\sigma,\uparrow}-\delta_{\sigma,\downarrow}}{4}$	$\frac{\sqrt{3}\delta_{\sigma,\downarrow}}{4}$	0	0
$\|\beta\sigma\rangle_{1_d}$	0	0	0	0	$\frac{\sqrt{3}\delta_{\sigma,\downarrow}}{4}$	$\frac{-2\delta_{\sigma,\uparrow}+\delta_{\sigma,\downarrow}}{4}$	0	0
$\|\alpha\sigma\rangle_{2_d}$	0	0	0	0	0	0	$\frac{-2\delta_{\sigma,\uparrow}-\delta_{\sigma,\downarrow}}{4}$	$\frac{-\sqrt{3}\delta_{\sigma,\downarrow}}{4}$
$\|\beta\sigma\rangle_{2_d}$	0	0	0	0	0	0	$\frac{-\sqrt{3}\delta_{\sigma,\downarrow}}{4}$	$\frac{-2\delta_{\sigma,\uparrow}+\delta_{\sigma,\downarrow}}{4}$

The spatial structure of the self-energy, which yields long-range spin and orbital order, is what opens the gap, by resolving spin and orbital degeneracy; the insulating state in LDA+U has therefore a very different nature than in DMFT.

To understand the nature of the difference, we consider the half-filled one-band Hubbard model (7) for a linear chain ($\varepsilon_k = -2\cos k_x a$) with lattice constant a. We double the unit cell (lattice constant $b = 2a$) and solve the model with Hartree-Fock, looking for long-range magnetic order. The mean-field Hamiltonian is

$$H^{\rm HF} = -t\sum_{\langle ii'\rangle\sigma} c^\dagger_{i\sigma}c_{i'\sigma} + U\sum_{i\sigma}\langle\hat{n}_{i\sigma}\rangle\hat{n}_{i-\sigma} - U\sum_i\langle\hat{n}_{i\uparrow}\rangle\langle\hat{n}_{i\downarrow}\rangle,$$

where $\langle\hat{n}_{i\uparrow}\rangle = 1/2 + m(-1)^i$, $\langle\hat{n}_{i\downarrow}\rangle = 1/2 - m(-1)^i$, and m is the magnetic moment per site. We set the Fermi level to zero and assume $m = 1/2$; the self-energy is $\Sigma_{i\sigma} = U\langle\hat{n}_{i-\sigma}\rangle$ and the

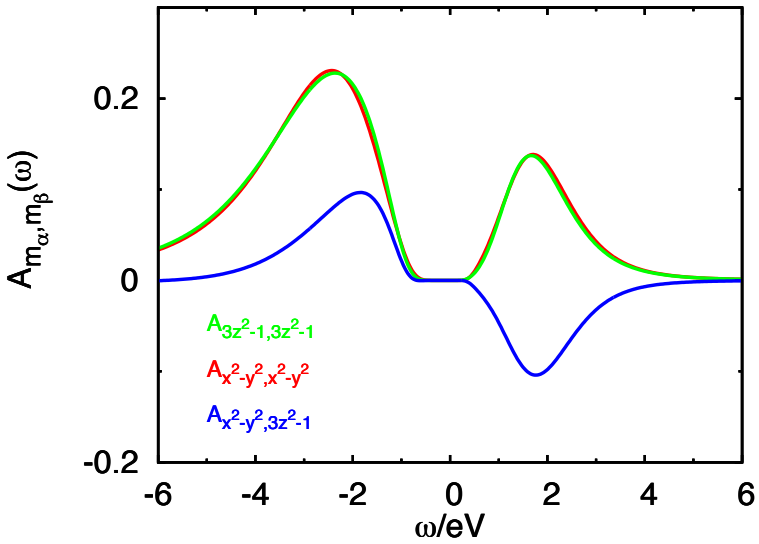

Fig. 7: *LDA+DMFT spectral matrix per spin (~ 230 K) in the orbitally-ordered paramagnetic phase of $KCuF_3$, cubic structure. Coulomb parameters: $U = 7$ eV, $J = 0.9$ eV. The off-diagonal terms, here large, are zero in the high temperature para-orbital phase.*

doubly degenerate eigenvectors are $\varepsilon_\pm = \pm\sqrt{\varepsilon_k^2 + U^2/4}$. At half-filling, only ε_- is occupied, and the gap opens at $k = \pi/2a$, the borders of the reduced BZ, $[-\pi/2a, \pi/2a)$. To compare with the DMFT solution of the one band Hubbard model, we unfold the bands back to the BZ of the small unit cell, $[-\pi/a, \pi/a)$. The Hartree-Fock bands can then be written as $\varepsilon_k + \Delta(k)$, where $\Delta(k) = -\varepsilon_k + [\Theta(\frac{\pi}{2a} - k) - \Theta(k - \frac{\pi}{2a})]\sqrt{\varepsilon_k^2 + U^2/4}$, and Θ is the step function. Thus, to obtain the Hartree-Fock bands we would have to correct the band energy ε_k with a function $\Delta(k)$ which has a jump at $k = \pi/2a$, i.e. a strong k-dependence. This should be compared with the divergence $\propto 1/\omega$ found in the real part of the $k-$independent DMFT self-energy for the paramagnetic half-filled Bethe lattice. Thus, the origin of the gap is completely different in statical and dynamical mean-field theory.

LDA+U has been successfully used to describe the magnetic ground state of many transition-metal compounds; however, since it is based on the static mean-field (Hartree-Fock-like) approximation, it often gives too large band gaps. A related problem is that the tendency to long-range order is overestimated, because fluctuation are neglected.

4.2 LDA+DMFT

The natural extension of LDA+U to include true correlation effects is LDA+DMFT [18–21]. In this approach we solve the Hubbard model $\hat{H}^{\rm LDA} + \hat{U}^l - \hat{H}^l_{\rm DC}$ by means of dynamical mean-field theory. To do this, first we map $\hat{H}^{\rm LDA} + \hat{U}^l - \hat{H}^l_{\rm DC}$ onto a multi-orbital Anderson model with the same Coulomb interaction at the impurity site; $\mathcal{G}(\omega)$ is the bath Green-function matrix of such Anderson model. Next, we label with i_c the correlated sites within the unit cell and with $lm\sigma$ the correlated orbitals at sites i_c; the local lattice Green-function matrix is

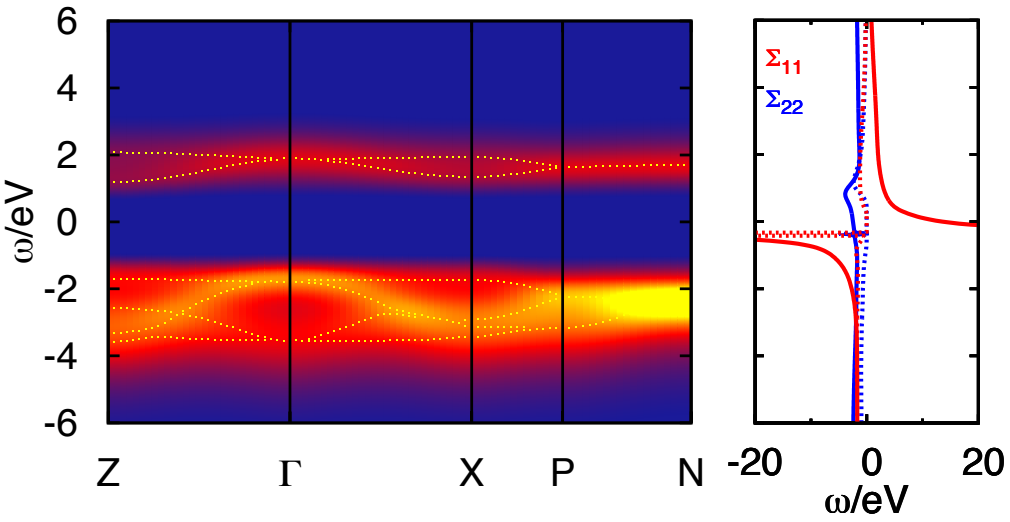

Fig. 8: *Left: LDA+DMFT correlated band structure (~ 230 K) in the orbitally-ordered phase of $KCuF_3$, cubic structure; the dots are the poles of the Green function. Right: Self-energy matrix in the basis of the natural orbitals. Full lines: real part. Dotted lines: imaginary part. Coulomb parameters: $U = 7$ eV, $J = 0.9$ eV.*

$$G_{i_c m\sigma, i'_c m'\sigma}(\omega) = \frac{1}{N_{\mathbf{k}}} \sum_{\mathbf{k}} \left(\left[\omega + \mu I - \hat{H}^{\rm LDA}_{\mathbf{k}} - \Sigma^l(\omega) + \hat{H}_{\rm DC} \right]^{-1} \right)_{i_c m\sigma, i'_c m'\sigma} .$$

The DMFT self-energy matrix $\Sigma^l(\omega)$ is non-zero in the correlated sector only; furthermore, it is diagonal in the site indices, $\Sigma^l_{i_c m\sigma, i'_c m'\sigma} = \delta_{i_c, i'_c} \Sigma^{i_c \sigma}_{m,m'}$. For two equivalent sites i_c and i'_c, space group symmetries transform $\Sigma^{i_c\sigma}_{m,m'}$ into $\Sigma^{i'_c\sigma}_{m,m'}$. In the paramagnetic case, in which $G_{i_c m\sigma, i'_c m'\sigma} = G_{i_c m\text{-}\sigma, i'_c m'\text{-}\sigma}$, the additional relation $\Sigma^{i'_c\sigma}_{m,m'} = \Sigma^{i'_c\text{-}\sigma}_{m,m'} = \Sigma^{i'_c}_{m,m'}$ holds.
Let us consider the example of paramagnetic $KCuF_3$. The primitive cell (Fig. 2) contains two formula units (and thus two equivalent Cu sites, labeled as 1 and 2 in Fig. 2). The LDA Hamiltonian which describes the e_g bands is a 4×4 matrix; the transformation between site 1 and 2 is $x, y, z \to y, x, -z$, and therefore $\Sigma^1_{\alpha\beta} = -\Sigma^2_{\alpha\beta}$, $\Sigma^1_{\alpha\alpha} = \Sigma^2_{\alpha\alpha}$, $\Sigma^1_{\beta\beta} = \Sigma^2_{\beta\beta}$. In matrix form

$$\begin{array}{c|cccc} \Sigma^l & |\alpha\sigma\rangle_1 & |\beta\sigma\rangle_1 & |\alpha\sigma\rangle_2 & |\beta\sigma\rangle_2 \\ |\alpha\sigma\rangle_1 & \Sigma^1_{\alpha\alpha} & \Sigma^1_{\alpha\beta} & 0 & 0 \\ |\beta\sigma\rangle_1 & \Sigma^1_{\beta\alpha} & \Sigma^1_{\beta\beta} & 0 & 0 \\ |\alpha\sigma\rangle_2 & 0 & 0 & \Sigma^1_{\alpha\alpha} & -\Sigma^1_{\alpha\beta} \\ |\beta\sigma\rangle_2 & 0 & 0 & -\Sigma^1_{\beta\alpha} & \Sigma^1_{\beta\beta} \end{array} .$$

The DMFT self-consistency condition requires that $G_{i_c, i_c}(\omega)$ equals the impurity Green-function matrix of the Anderson model, $G(\omega)$. Thus, in the paramagnetic case

$$G_{m,m'}(\omega) = G_{i_c m\sigma, i_c m'\sigma}(\omega), \quad \mathcal{G}^{-1}_{m,m'}(\omega) = G^{-1}_{m,m'}(\omega) + \Sigma^{i_c}_{m,m'}(\omega).$$

The site i_c is one of the equivalent sites $\{i_c\}$; in the $KCuF_3$ example, it could be, e.g., a site 1.
The solution of the multi-orbital quantum-impurity model requires a method which can deal with realistic Coulomb interactions and Green-function matrices; depending on the problem we want to address, we can choose from quantum Monte Carlo [7, 8], Lanczos [9], the numerical renormalization group, and many more.
The Hirsch-Fye QMC [7] approach, presented in the Lecture of Nils Blümer, is very general; a limitation is that spin-flip and pair-hopping processes yield a strong sign problem, and have to be neglected; in many cases this is, however, a good approximation. In Fig. 7 we show the *paramagnetic* e_g spectral-function matrix of $KCuF_3$ at ~ 230 K, calculated with a Hirsch-Fye QMC solver. The figure shows that with DMFT we can obtain an insulating orbitally ordered solution even in the absence of long-range magnetic order; this is not the case in static mean-field theory. The off-diagonal elements of the spectral matrix (and correspondingly those of the self-energy matrix) are large and cannot be neglected. In Fig. 8 we show the LDA+DMFT e_g band structure of $KCuF_3$, corresponding to the spectral matrix in Fig. 7. We can compare these bands with the static mean-field *antiferromagnetic* band structure in Fig. 6. The LDA+DMFT band gap is significantly smaller. The imaginary part of the self-energy, which is zero in static mean-field theory, makes the Hubbard bands partly incoherent. The real part of the self-energy of the half-filled orbital (Fig. 8), which in static mean-field theory does not depend on ω, diverges at low frequencies, as in the case of the half-filled Bethe lattice.
The continuous-time QMC technique [8], discussed in the Lecture of Philipp Werner, allows us to include in our model spin-flip and pair-hopping terms. As an example we present LDA+DMFT results for Ca_2RuO_4 (Fig. 9), a layered $4d^4$ perovskite which at low energy can be described by a t_{2g} Hubbard model of the form (14); to solve it we use the weak-coupling continuous-time QMC scheme. Fig. 9 shows that neglecting spin-flip and pair-hopping terms changes the degeneracy of multiplets, and leads to an overestimation of the mass renormalization m^*/m [22].

The LDA+DMFT self-consistent procedure works as follows (for QMC solvers $\omega \to i\omega_n$)

- construct $\hat{H}^{\mathrm{LDA}} + \hat{U}^l - \hat{H}^l_{\mathrm{DC}}$
- calculate the local Green-function matrix for a starting self-energy matrix

$$G_{i_c\sigma,i_c\sigma}(\omega) = \frac{1}{N_{\mathbf{k}}} \sum_{\mathbf{k}} \left([\omega - \hat{H}^{\mathrm{LDA}}_{\mathbf{k}} - \Sigma^l(\omega) + \mu I + \hat{H}^l_{\mathrm{DC}}]^{-1} \right)_{i_c\sigma,i_c\sigma} .$$

  For equivalent sites, the LDA Hamiltonian and the self-energy matrix should transform according to space-group symmetries.

- calculate the bath Green-function matrix

$$\mathcal{G}^{-1}(\omega) = G^{-1}(\omega) + \Sigma(\omega), \quad G(\omega) = G_{i_c\sigma,i_c\sigma}(\omega)$$

- obtain the impurity Green-function matrix $G(\omega)$ by solving the quantum-impurity problem defined by $\mathcal{G}(\omega)$ and the Coulomb interaction $\hat{U}^l$ at sites $\{i_c\}$

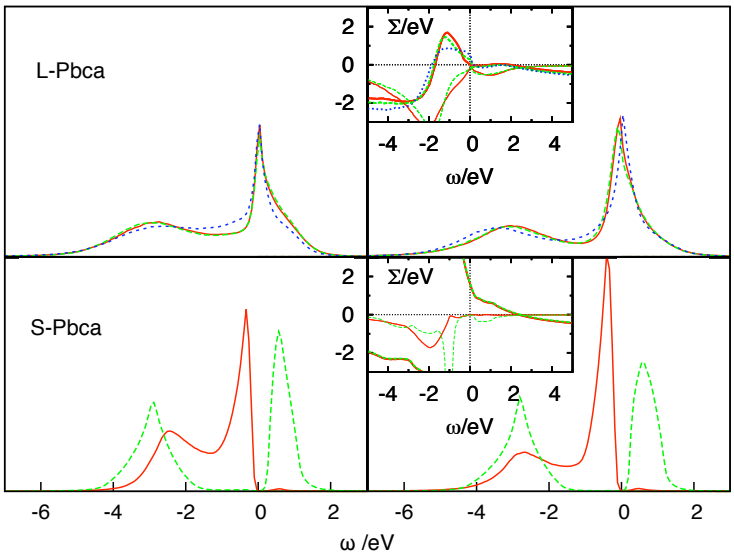

Fig. 9: *Ca_2RuO_4: t_{2g} spectral functions in the high-temperature L-Pbca phase and in the low temperature S-Pbca phase. Left: without spin-flip and pair-hopping terms. Right: with spin-flip and pair-hopping terms. Red: xy. Green and blue: xz and yz. From Ref. [22].*

- calculate the self-energy matrix

$$\Sigma(\omega) = \mathcal{G}^{-1}(\omega) - G^{-1}(\omega)$$

- check if self-consistency is reached; if not, recalculate $G_{i_c\sigma,i_c\sigma}(\omega)$ and start over again.

In LDA+DMFT the double-counting correction is the same as in LDA+U; in the case of massive downfolding to the correlated-electron sector, as previously discussed, it is incorporated in the chemical potential and does not need to be calculated explicitly.

The extension of LDA+DMFT to the spin-polarized case (spin-dependent self-energy matrix and Green-function matrices) is straightforward. Long-range anti-ferromagnetic order can also be treated, provided that we use the appropriate unit cell. Let us consider the case of $KCuF_3$. Below T_N this system is antiferromagnetic along **z** and ferromagnetic in the xy plane. To account for this magnetic order, we have to use a unit cell with 4 formula units, the same that we used for the LDA+U example; the self-energy matrix has therefore the same spatial structure as in LDA+U

$\Sigma^{l\sigma}$	$\lvert\alpha\sigma\rangle_{1_u}$	$\lvert\beta\sigma\rangle_{1_u}$	$\lvert\alpha\sigma\rangle_{2_u}$	$\lvert\beta\sigma\rangle_{2_u}$	$\lvert\alpha\sigma\rangle_{1_d}$	$\lvert\beta\sigma\rangle_{1_d}$	$\lvert\alpha\sigma\rangle_{2_d}$	$\lvert\beta\sigma\rangle_{2_d}$
$\lvert\alpha\sigma\rangle_{1_u}$	$\Sigma^{1\sigma}_{\alpha\alpha}$	$\Sigma^{1\sigma}_{\alpha\beta}$	0	0	0	0	0	0
$\lvert\beta\sigma\rangle_{1_u}$	$\Sigma^{1\sigma}_{\beta\alpha}$	$\Sigma^{1\sigma}_{\beta\beta}$	0	0	0	0	0	0
$\lvert\alpha\sigma\rangle_{2_u}$	0	0	$\Sigma^{1\sigma}_{\alpha\alpha}$	$-\Sigma^{1\sigma}_{\alpha\beta}$	0	0	0	0
$\lvert\beta\sigma\rangle_{2_u}$	0	0	$-\Sigma^{1\sigma}_{\beta\alpha}$	$\Sigma^{1\sigma}_{\beta\beta}$	0	0	0	0
$\lvert\alpha\sigma\rangle_{1_d}$	0	0	0	0	$\Sigma^{1\text{-}\sigma}_{\alpha\alpha}$	$\Sigma^{1\text{-}\sigma}_{\alpha\beta}$	0	0
$\lvert\beta\sigma\rangle_{1_d}$	0	0	0	0	$\Sigma^{1\text{-}\sigma}_{\beta\alpha}$	$\Sigma^{1\text{-}\sigma}_{\beta\beta}$	0	0
$\lvert\alpha\sigma\rangle_{2_d}$	0	0	0	0	0	0	$\Sigma^{1\text{-}\sigma}_{\alpha\alpha}$	$-\Sigma^{1\text{-}\sigma}_{\alpha\beta}$
$\lvert\beta\sigma\rangle_{2_d}$	0	0	0	0	0	0	$-\Sigma^{1\text{-}\sigma}_{\beta\alpha}$	$\Sigma^{1\text{-}\sigma}_{\beta\beta}$.

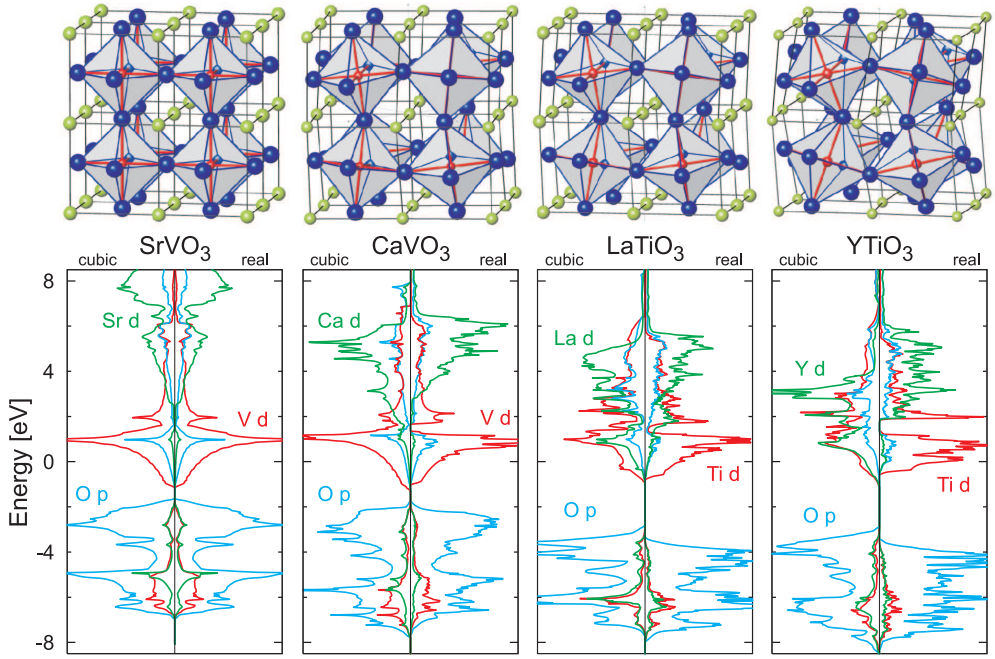

Fig. 10: *Evolution of crystal structure and LDA band structure in the series of $3d^1$ perovskites with the $GdFeO_3$-type distortion. From Ref. [12].*

The LDA+DMFT scheme can be easily extended to treat clusters, by using a supercell and treating the supercell as impurity; alternative extensions to account for the **k** dependence of the self-energy are the dynamical-cluster approximation (DCA) [23], the dual-fermion approach, or GW+DMFT. Some of these methods will be discussed in the Lectures of Sasha Lichtenstein and Karsten Held. Finally, LDA+DMFT, as LDA+U, can be also made charge self-consistent. This requires to work, as in LDA+U, with the full Hamiltonian and to account explicitly for the double-counting correction.

The calculation of the screened Coulomb parameters is a major open problem, in LDA+DMFT as in LDA+U. In the absence of a definitive method, a useful approach is to analyze trends in similar materials, to single out the effects of chemistry and structural distortions from those of the Coulomb interaction. We adopt this approach in Ref. [24] to study the Mott transition in the series of $3d^1$ ($t_{2g}^1 e_g^0$) perovskites. These materials all have the $GdFeO_3$-type structure, with distortions (tilting, rotation, deformation of the cation cage) that increase along the series (Fig. 10). By means of massive downfolding based on the NMTO method [12], we obtain the material-specific t_{2g} Wannier basis (crystal-field orbitals) shown in Fig. 5. With increasing distortions, the t_{2g} band-width decreases and the crystal-field splitting increases, reaching $\sim$ 300 meV in $YTiO_3$, still a small fraction of the t_{2g} band width. We find that, despite of its small value, the crystal-field splitting plays a crucial role in helping the metal-insulator transition, by reducing the orbital degeneracy [25] of the many-body states and favoring the formation of an orbitally-ordered state.

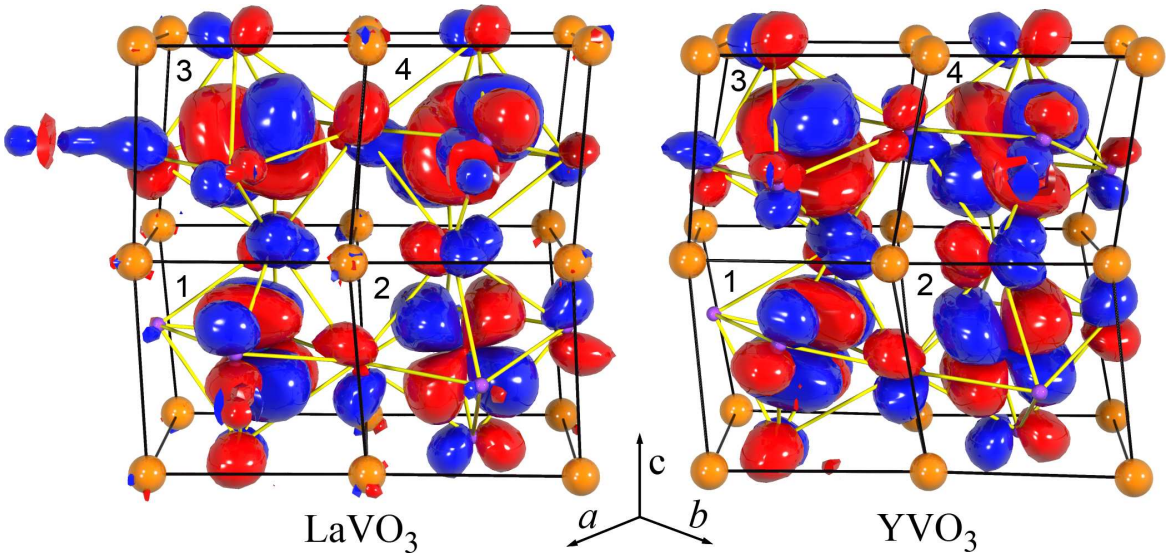

Fig. 11: *Orbital-order (empty orbital) in the $3d^2$ perovskites $LaVO_3$ and YVO_3. From Ref. [26].*

5 The origin of orbital order

In this Section we will show an example of how LDA+DMFT can be used as a tool to understand physical phenomena. Orbital order is believed to play a crucial role in determining the electronic and magnetic properties of many transition-metal compounds. Still, the origin of orbital order in real materials is a subject of hot debate.

The hallmark of orbital order is the co-operative Jahn-Teller distortion. A paradigmatic example is $KCuF_3$. The co-operative Jahn-Teller distortion is shown in Fig. 2. This static distortion gives rise to a crystal field, which splits the otherwise degenerate e_g doublet. LDA+DMFT calculations have proven that, due to Coulomb repulsion, even a crystal-field splitting much smaller than the band width can lead to orbital order. The importance of such effect for real materials has been realized first for $LaTiO_3$ and $YTiO_3$ [24, 12]. The same effect is at work in a number of other systems with different electronic structure. We discuss few cases. In $3d^2$ vanadates [26] the t_{2g} crystal-field splitting is even smaller than in $3d^1$ perovskites. Still, orbital fluctuations are already strongly suppressed at room temperature, yielding the orbital-order shown in Fig. 11. In Ca_2RuO_4, due to the layered perovskite structure, the 2/3-filled t_{2g} bands split into a wide xy and two narrow xz and yz bands. In the low-temperature phase (S-Pbca) the system is an insulator with a small gap and exhibits xy-orbital order: at each site the xy orbital is filled with two electrons. Above 350 K, in the L-Pbca phase, Ca_2RuO_4 is metallic and no orbital order has been reported. We find (Fig. 9) that the metal-insulator transition is driven by the structural L-Pbca $\rightarrow$ S-Pbca phase transition; furthermore, in the insulating phase the $\sim$ 300 meV crystal-field splitting overcomes the band missmatch and we find xy orbital order [22]. The case of $3d^9$ $KCuF_3$ and $3d^4$ $LaMnO_3$ is even more extreme: the e_g crystal-field splitting is $\sim 0.5-1$ eV at 300 K; with such a large splitting, orbital fluctuations are suppressed up to melting temperature.

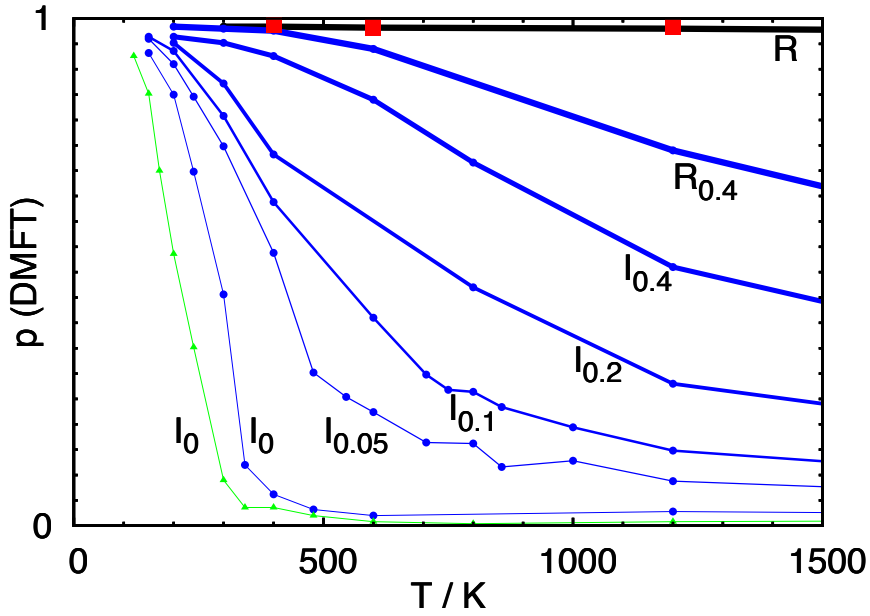

Fig. 12: *Orbital order transition in $KCuF_3$. Orbital polarization p as a function of temperature calculated in LDA+DMFT. R: $U = 7$ eV, experimental structure. Circles: $U = 7$ eV, idealized structures R_δ and I_δ with decreasing crystal-field. Triangles: $U = 9$ eV, I_0 only. Squares: two-sites CDMFT. From Ref. [4].*

Orbital order can already arise, however, in the absence of static distortions. In a seminal work, Kugel and Khomskii [27] showed that in strongly-correlated systems with orbital degrees of freedom (degenerate e_g or t_{2g} levels), many-body effects can give rise to orbital order via a purely electronic mechanism (*spin and orbital super-exchange*). In this picture, the co-operative Jahn-Teller distortion (and thus the crystal-field splitting) is a consequence of orbital order. In the opposite scenario, the co-operative Jahn-Teller distortion is due to the electron-phonon coupling, which removes orbital degeneracy, and orbital order is driven by the static distortion, as discussed above. We analyze these two scenarios for $KCuF_3$ and $LaMnO_3$, the text-book examples [28] of orbitally-ordered systems. LDA+U total energy calculations show [15, 29] that in these systems the co-operative Jahn-Teller distortion is stabilized by U, a result recently confirmed in LDA+DMFT [30]. This could indicate that super-exchange is the driving mechanism. However, if this is the case it is hard to explain why the magnetic transition temperature, determined by super-exchange, is much lower than the orbital-order transition temperature: $T_N \sim 40$ K for $KCuF_3$ and $T_N \sim 140$ K for $LaMnO_3$, while the co-operative Jahn-Teller distortion persists up to 1000 K or more.

$LaMnO_3$ and $KCuF_3$ can both be described by a two-band e_g Hubbard model. In the case of $LaMnO_3$ we have additionally to take into account the Hund's rule coupling between e_g electrons and t_{2g} spins, $\mathbf{S}_{t_{2g}}$. Thus the minimal model to understand orbital order in these two

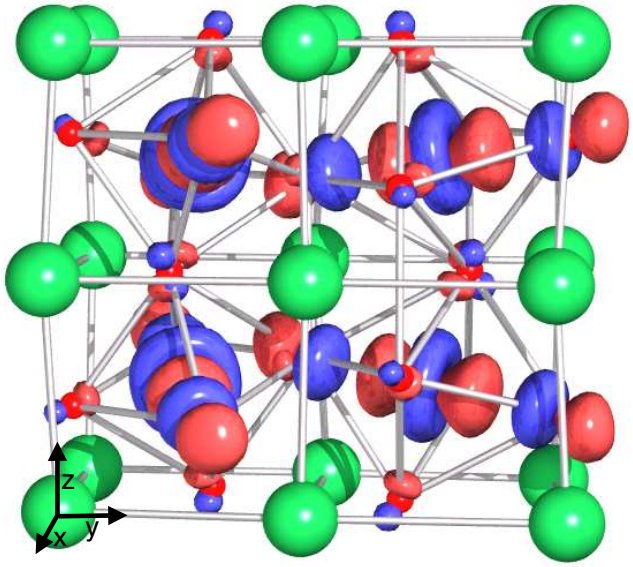

Fig. 13: *Orbital order (LDA+DMFT calculations) in the rare-earth perovskite $TbMnO_3$ with the $GdFeO_3$-type structure. From Ref. [32]. This system has the same structure of $LaMnO_3$.*

systems is the Hamiltonian [31]

$$H = - \sum_{im\sigma,i'm'\sigma'} t^{i,i'}_{m,m'} u^{i,i'}_{\sigma,\sigma'} c^\dagger_{im\sigma} c_{i'm'\sigma'} - h \sum_{im} (\hat{n}_{im\uparrow} - \hat{n}_{im\downarrow}) + U \sum_{im} \hat{n}_{im\uparrow}\hat{n}_{im\downarrow} + \frac{1}{2} \sum_{im(\neq m')\sigma\sigma'} (U - 2J - J\delta_{\sigma,\sigma'}) \hat{n}_{im\sigma}\hat{n}_{im'\sigma'} \; .$$

Here $m, m' = 3z^2 - r^2, x^2 - y^2$. The local magnetic field $h = JS_{t_{2g}}$ describes the Hund's rule coupling to t_{2g} electrons, and $u_{i\sigma,i'\sigma'} = 2/3(1 - \delta_{i,i'})$ accounts for the disorder in orientation of the t_{2g} spins. In the case of $KCuF_3$ $u_{i\sigma,i'\sigma'} = \delta_{\sigma,\sigma'}$ and $h = 0$. For the Coulomb parameters we use the theoretical estimates $J = 0.9$ eV ($KCuF_3$) and $J = 0.75$ eV ($LaMnO_3$) and vary U around 5 eV ($LaMnO_3$) and 7 eV ($KCuF_3$). In the high-spin regime, our results are not very sensitive to h; we show results for $h \sim 1.3$ eV. We use the massive downfolding technique based on the NMTO method to calculate hopping integrals and crystal-field splittings.

To single out the effects of many-body super-exchange (Kugel-Khomksii mechanism) from the effect of the crystal-field splitting, we perform LDA+DMFT and LDA+CDMFT calculations for a series of hypothetical structures, in which the distortions (and thus the crystal-field splitting) are progressively reduced. In the case of $KCuF_3$, these hypothetical structures are shown in Fig. 2, and the corresponding e_g bands are shown in Fig. 8. For each structure we calculate the order parameter, the orbital polarization p, defined as the difference in the occupations of natural orbitals. In Fig. 12 we show p as a function of temperature. For the experimental structure, $p(T) \sim 1$ till melting temperature; this means that, if the structure stays the same, the system remains orbitally ordered till the crystal melts. The empty orbitals on different sites make the pattern shown in Fig. 2. For the ideal cubic structure I_0, we find that $p(T) = 0$ at high temperature, but a transition occurs at $T_{\rm KK} \sim 350$ K. This $T_{\rm KK}$ is the critical temperature

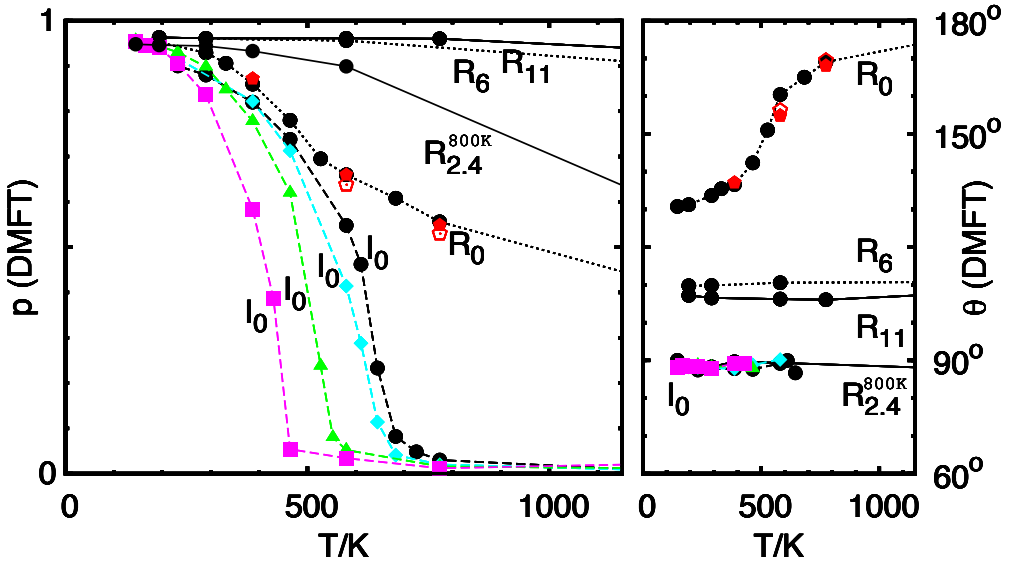

Fig. 14: *Orbital order transition in $LaMnO_3$. Orbital polarization p (left) and (right) occupied state $|\theta\rangle = \cos\frac{\theta}{2}|3z^2 - r^2\rangle + \sin\frac{\theta}{2}|x^2 - y^2\rangle$ as a function of temperature. Solid line: 300 K experimental structure (R_{11}) and 800 K experimental structure. Dots: orthorhombic structures with half (R_6) or no (R_0) Jahn-Teller distortion. Pentagons: 2 (full) and 4 (empty) sites CDMFT. Dashes: ideal cubic structure (I_0). Circles: $U = 5$ eV. Diamonds: $U = 5.5$ eV. Triangles: $U = 6$ eV. Squares: $U = 7$ eV. Crystal field splittings (meV): 840 (R_{11}), 495 (R_6), 168 ($R_{2.4}^{800\ K}$), and 0 (I_0). From Ref. [33].*

in the absence of Jahn-Teller effect. Our result shows that around 350 K super-exchange could drive alone the co-operative Jahn-Teller distortion. However, experimentally, the co-operative Jahn-Teller distortion persists up to 800 K or even higher temperature. $T_{\rm KK}$, although large, is not large enough to explain the presence of a co-operative Jahn-Teller distortion above 350 K; electron-phonon interaction plays a key role. Fig. 12 shows that a ~ 200 meV crystal-field (as in the ideal $R_{0.4}$, which has a Jahn-Teller distortion $\sim 10\%$ of the experimental structure) yields already an almost complete suppression of orbital fluctuations up to at least 1500 K.

In the case of $LaMnO_3$ we find (see Fig. 14) $T_{\rm KK} \sim 700$ K. However, besides the co-operative Jahn-Teller distortion and tetragonal compression, $LaMnO_3$ exhibits a $GdFeO_3$-type distortion (Fig. 13), which tends to reduce the e_g band-width [12]. Thus we study in addition an ideal structure R_0 with all distortions except the Jahn-Teller. For such system we cannot obtain $T_{\rm KK}$ from $p(T)$, because, due to the crystal-field splitting ~ 200 meV, Coulomb repulsion strongly suppress orbital fluctuations even at 1500 K. Instead, we study the evolution of the occupied orbital $|\theta\rangle = \cos\frac{\theta}{2}|3z^2 - r^2\rangle + \sin\frac{\theta}{2}|x^2 - y^2\rangle$ with temperature. For the experimental structure (R_{11}) we find $\theta \sim 108^o$, in agreement with experiments, and for the I_0 structure we obtain $\theta = 90^o$. For the R_0 structure we find two regimes. At high temperature the occupied orbital is the lower energy crystal-field orbital ($\theta = 180^o$). At $T_{\rm KK} \sim 550$ K super-exchange rotates this θ towards 90^o, reaching 130^0 in the zero temperature limit. Such $T_{\rm KK}$ is still very large, but again not sufficient to explain that the Jahn-Teller distortion persist in nanoclusters up to

melting temperature [34]. Thus, as for $KCuF_3$, electron-lattice coupling is essential to explain the co-operative Jahn-Teller distortion at high temperature.
Although the co-operative Jahn-Teller distortion persists in domains up to melting temperature, a order-to-disorder (or *orbital melting*) transition has been reported at $T_{\rm OO} \sim 750$ K [35]. Since $T_{\rm KK} \sim T_{\rm OO}$, super-exchange could play a crucial role in such transition. To resolve this issue, we analyze a series of materials for which $T_{\rm OO}$ has been measured: rare-earth manganites with structures similar to $LaMnO_3$. For this series, it has been reported that $T_{\rm OO}$ strongly increases with decreasing the rare-earth radius, reaching about 1500 K in $TbMnO_3$. Instead, with LDA+DMFT and actually find the opposite trend: $T_{\rm KK}$ is maximum in $LaMnO_3$ and slightly decreases along the series. Taking the tetragonal crystal-field into account reduces $T_{\rm KK}$, further increasing the discrepancies with experiment. This proves that, surprisingly, super-exchange effects, although very efficient, in the light of the experimentally reported trends, play a minor role for the orbital order melting observed in rare earth manganites [32].

6 Conclusions

The many-body problem is central to theoretical solid-state physics. Density functional theory is the standard approach for describing the electronic properties of materials. It is a very successful method, which allows us to understand and predict the properties of many systems. However, DFT practice fails completely for *strongly-correlated* materials, in which the movement of one electron depends on the actual, not only the mean position of all other electrons, since it has to avoid their Coulomb repulsion. In this Lecture we have seen a successful scheme to deal with strongly-correlated systems: LDA+DMFT. It is based on the separation of electrons into correlated and uncorrelated. While for uncorrelated electrons we use standard methods based on density-functional theory, for correlated electrons we build material-specific many-body models and solve them with DMFT. Building models requires the construction of localized and material-specific basis sets. To this end, various successful approaches have been devised, such as the *ab-initio* downfolding technique, maximally-localized Wannier functions and projectors. Material-specific many-body models are however complex. Solving them with DMFT requires flexible and efficient quantum-impurity solvers. Examples are Hirsch-Fye QMC, continuous-time QMC, and Lanczos. Short and/or long range spatial correlations can be in principle accounted for within different methods: CDMFT, DCA, dual fermions, GW+DMFT. Thanks to the improvements of impurity solvers and to modern supercomputers, we have been able to include in LDA+DMFT calculations more degrees of freedom, to reach experimental temperatures, to calculate properties beyond the spectral function, and to move towards predictive power. From the many successful applications of LDA+DMFT we have learned that *details do matter*; for example a crystal-field splitting of merely hundred meV, typically neglected in studies based on simple model Hamiltonians, plays a crucial role in stabilizing the orbitally-ordered Mott insulating state [24], and super-exchange, although very efficient, is not the driving mechanism of orbital order in the text-book examples of actual orbitally-ordered materials, $LaMnO_3$ and $KCuF_3$.

Much work lies ahead. A general and effective quantum-impurity solver is not yet available; effective **k**-dependent extensions of LDA+DMFT are under development. Central to the success of LDA+DMFT and its extensions is the separation of electrons into light and heavy. This separation, however, is also the main source of trouble. The double-counting correction is essentially unknown. To account for screening effects in a realistic setting is very difficult. Furthermore, by truncating the Coulomb interaction outside the correlated sector, we assume implicitly that the effect of many-body downfolding to the correlated sector is *only* screening; effects which go beyond the mere Coulomb renormalization are usually neglected. Ultimately, these approximations have to be put to a test.

Finally, we have to remember that many-body phenomena are emergent behaviors [36]. Each of such phenomena, although in principle described by the same many-body Hamiltonian (1), the *theory of almost everything* [37], may have a very different nature. To predict new phenomena before they are observed is therefore extremely challenging. After they are discovered, they are often elusive and might remain mysterious for decades, like it is happening for high-temperature superconductivity. In developing *ab-initio* theories for strongly-correlated systems, we have thus always to keep in mind that the crucial aspect to explain a given phenomenon might be hidden in some detail which in more ordinary circumstances would play no role. The challenge is thus to identify *which* details do matter.

Acknowledgment

Support of the Deutsche Forschungsgemeinschaft through FOR1346 is gratefully acknowledged.

Appendices

A Constants and units

In this Lecture, formulas are written in atomic units. The unit of mass m_0 is the electron mass ($m_0 = m_e$), the unit of charge e_0 is the electron charge ($e_0 = e$), the unit of length a_0 is the Bohr radius ($a_0 = a_B \sim 0.52918$ = Å), and the unit of time is $t_0 = 4\pi\varepsilon_0\hbar a_0/e^2$. In these units, m_e, a_B, e and $1/4\pi\varepsilon_0$ have the numerical value 1; the speed of light is $c = 1/\alpha \sim 137$ in atomic units. The unit of energy is $1Ha = e^2/4\pi\varepsilon_0 a_0 \sim 27.211$ eV. These are the natural units for theory. When comparing to experiments, for convenience, we give the energies in eV or meV.

B Atomic orbitals

B.1 Radial functions

The nlm hydrogen-like atomic orbital is given by

$$\psi_{nlm}(\rho,\theta,\phi) = R_{nl}(\rho)Y_l^m(\theta,\phi),$$

where $R_{nl}(\rho)$ is the radial function and $Y_m^l(\theta,\phi)$ a spherical harmonic, $\rho = Zr$ and Z the atomic number. In atomic units, the radial functions are

$$R_{nl}(\rho) = \sqrt{\left(\frac{2Z}{n}\right)^3 \frac{(n-l-1)!}{2n[(n+l)!]^3}} e^{-\rho/n} \left(\frac{2\rho}{n}\right)^l L_{n-l-1}^{2l+1}\left(\frac{2\rho}{n}\right),$$

where L_{n-l-1}^{2l+1} are generalized Laguerre polynomials of degree $n-l-1$.
The radial function for $n = 1, 2, 3$ are

$$\begin{aligned}
R_{1s}(\rho) &= 2 \quad Z^{3/2} && e^{-\rho} \\
R_{2s}(\rho) &= \tfrac{1}{2\sqrt{2}} \quad Z^{3/2} && (2-\rho)\, e^{-\rho/2} \\
R_{2p}(\rho) &= \tfrac{1}{2\sqrt{6}} \quad Z^{3/2} && \rho\, e^{-\rho/2} \\
R_{3s}(\rho) &= \tfrac{2}{3\sqrt{3}} \quad Z^{3/2} && (1-2\rho/3+2\rho^2/27)\, e^{-\rho/3} \\
R_{3p}(\rho) &= \tfrac{4\sqrt{2}}{9\sqrt{3}} \quad Z^{3/2} && \rho(1-\rho/6)\, e^{-\rho/3} \\
R_{3d}(\rho) &= \tfrac{2\sqrt{2}}{81\sqrt{15}} \quad Z^{3/2} && \rho^2\, e^{-\rho/3}
\end{aligned}$$

where we used the standard notation s for $l = 0$, p for $l = 1$ and d for $l = 2$.

B.2 Real harmonics

To study solids, it is usually convenient to work in the basis of real harmonics. The latter are defined in terms of the spherical harmonics as follows:

$$y_{l0} = Y_0^l, \quad y_{lm} = \frac{1}{\sqrt{2}}(Y_{-m}^l + (-1)^m Y_m^l), \quad y_{l-m} = \frac{i}{\sqrt{2}}(Y_{-m}^l - (-1)^m Y_m^l), \quad m > 0.$$

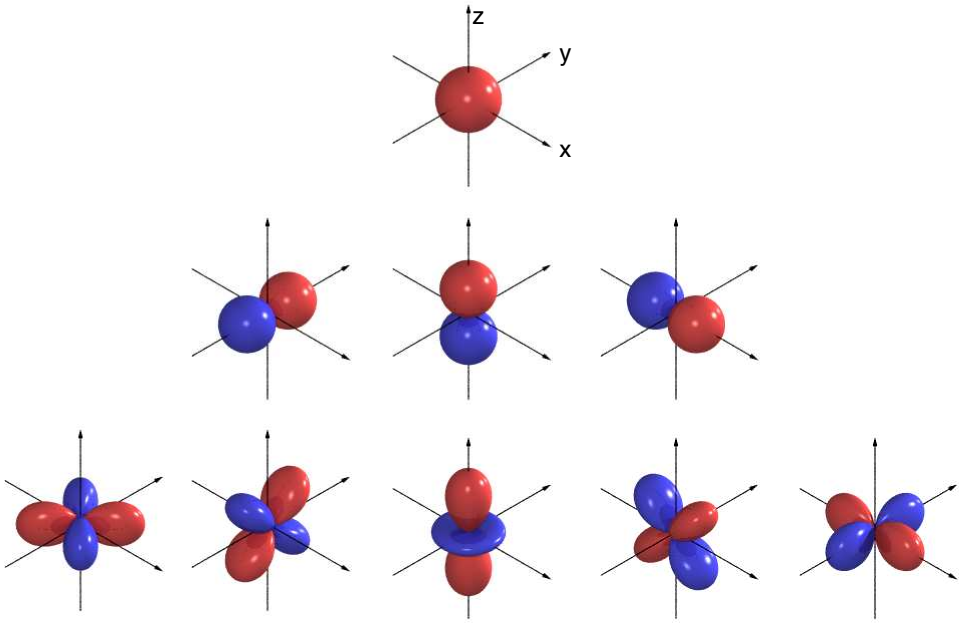

Fig. 15: *The s (first row), p_y, p_z, p_x (second row), and d_{xy}, d_{yz}, $d_{3z^2-r^2}$, d_{xz}, $d_{x^2-y^2}$ (last row) real harmonics.*

Using the definitions $x = r\sin\theta\cos\phi$, $y = r\sin\theta\sin\phi$, $z = r\cos\theta$, we can express the $l = 0, 1, 2$ real harmonics (Fig. 15) as

$$
\begin{aligned}
s &= y_{00} = Y_0^0 &&= \sqrt{\tfrac{1}{4\pi}} \\
p_y &= y_{1-1} = \tfrac{i}{\sqrt{2}}(Y_1^1 + Y_{-1}^1) &&= \sqrt{\tfrac{3}{4\pi}}\, y/r \\
p_z &= y_{10} = Y_2^0 &&= \sqrt{\tfrac{3}{4\pi}}\, z/r \\
p_x &= y_{11} = \tfrac{1}{\sqrt{2}}(Y_1^1 - Y_{-1}^1) &&= \sqrt{\tfrac{3}{4\pi}}\, x/r \\
d_{xy} &= y_{2-2} = \tfrac{i}{\sqrt{2}}(Y_2^2 - Y_{-2}^2) &&= \sqrt{\tfrac{15}{4\pi}}\, xy/r^2 \\
d_{yz} &= y_{2-1} = \tfrac{i}{\sqrt{2}}(Y_1^2 + Y_{-1}^2) &&= \sqrt{\tfrac{15}{4\pi}}\, yz/r^2 \\
d_{3z^2-r^2} &= y_{20} = Y_2^0 &&= \sqrt{\tfrac{15}{4\pi}}\tfrac{1}{2\sqrt{3}}\,(3z^2 - r^2)/r^2 \\
d_{xz} &= y_{21} = \tfrac{1}{\sqrt{2}}(Y_1^2 - Y_{-1}^2) &&= \sqrt{\tfrac{15}{4\pi}}\, xz/r^2 \\
d_{x^2-y^2} &= y_{22} = \tfrac{1}{\sqrt{2}}(Y_2^2 + Y_{-2}^2) &&= \sqrt{\tfrac{15}{4\pi}}\tfrac{1}{2}\,(x^2 - y^2)/r^2
\end{aligned}
$$

B.3 Slater-Koster integrals

The interatomic Slater-Koster two-center integrals are defined as

$$E_{lm,l'm'} = \int d\mathbf{r}\, \overline{\psi}_{lm}(\mathbf{r}-\mathbf{d}) V(\mathbf{r}-\mathbf{d}) \psi_{l'm'}(\mathbf{r}).$$

They can be expressed as a function of radial integrals $V_{ll'\alpha}$, which scale with the distance d roughly as $d^{-(l+l'+1)}$ [38], and direction cosines, defined as

$$l = \mathbf{d}\cdot\hat{x}/d, \quad m = \mathbf{d}\cdot\hat{y}/d, \quad n = \mathbf{d}\cdot\hat{z}/d.$$

The Slater-Koster integrals for s, p, and d orbitals [38] are listed below.

$E_{s,s}$	=	$V_{ss\sigma}$		
$E_{s,x}$	=	$lV_{sp\sigma}$		
$E_{x,x}$	=	$l^2V_{pp\sigma}$	$+(1-l^2)V_{pp\pi}$	
$E_{x,y}$	=	$lmV_{pp\sigma}$	$-lmV_{pp\pi}$	
$E_{x,z}$	=	$lnV_{pp\sigma}$	$-lnV_{pp\pi}$	
$E_{s,xy}$	=	$\sqrt{3}lmV_{sd\sigma}$		
E_{s,x^2-y^2}	=	$\frac{1}{2}\sqrt{3}(l^2-m^2)V_{sd\sigma}$		
$E_{s,3z^2-r^2}$	=	$[n^2-\frac{1}{2}(l^2+m^2)]V_{sd\sigma}$		
$E_{x,xy}$	=	$\sqrt{3}l^2mV_{pd\sigma}$	$+m(1-2l^2)V_{pd\pi}$	
$E_{x,yz}$	=	$\sqrt{3}lmnV_{pd\sigma}$	$-2lmnV_{pd\pi}$	
$E_{x,zx}$	=	$\sqrt{3}l^2nV_{pd\sigma}$	$+n(1-2l^2)V_{pd\pi}$	
E_{x,x^2-y^2}	=	$\frac{\sqrt{3}}{2}l[(l^2-m^2)]V_{pd\sigma}$	$+l(1-l^2+m^2)V_{pd\pi}$	
E_{y,x^2-y^2}	=	$\frac{\sqrt{3}}{2}m[(l^2-m^2)]V_{pd\sigma}$	$-m(1+l^2-m^2)V_{pd\pi}$	
E_{z,x^2-y^2}	=	$\frac{\sqrt{3}}{2}n[(l^2-m^2)]V_{pd\sigma}$	$-n(l^2-m^2)V_{pd\pi}$	
$E_{x,3z^2-r^2}$	=	$l[n^2-\frac{1}{2}(l^2+m^2)]V_{pd\sigma}$	$-\sqrt{3}ln^2V_{pd\pi}$	
$E_{y,3z^2-r^2}$	=	$m[n^2-\frac{1}{2}(l^2+m^2)]V_{pd\sigma}$	$-\sqrt{3}mn^2V_{pd\pi}$	
$E_{z,3z^2-r^2}$	=	$n[n^2-\frac{1}{2}(l^2+m^2)]V_{pd\sigma}$	$+\sqrt{3}n(l^2+m^2)V_{pd\pi}$	
$E_{xy,xy}$	=	$3l^2m^2V_{dd\sigma}$	$+(l^2+m^2-4l^2m^2)V_{dd\pi}$	$+(n^2+l^2m^2)V_{dd\delta}$
$E_{xy,yz}$	=	$3lm^2nV_{dd\sigma}$	$+ln(1-4m^2)V_{dd\pi}$	$+ln(m^2-1)V_{dd\delta}$
$E_{xy,zx}$	=	$3l^2mnV_{dd\sigma}$	$+mn(1-4l^2)V_{dd\pi}$	$+mn(l^2-1)V_{dd\delta}$
E_{xy,x^2-y^2}	=	$\frac{3}{2}lm(l^2-m^2)V_{dd\sigma}$	$2lm(m^2-l^2)V_{dd\pi}$	$\frac{1}{2}lm(l^2-m^2)V_{dd\delta}$
E_{yz,x^2-y^2}	=	$\frac{3}{2}mn(l^2-m^2)V_{dd\sigma}$	$-mn[1+2(l^2-m^2)]V_{dd\pi}$	$+mn[1+\frac{1}{2}(l^2-m^2)]V_{dd\delta}$
E_{zx,x^2-y^2}	=	$\frac{3}{2}nl(l^2-m^2)V_{dd\sigma}$	$+nl[1-2(l^2-m^2)]V_{dd\pi}$	$-nl[1-\frac{1}{2}(l^2-m^2)]V_{dd\delta}$
$E_{xy,3z^2-r^2}$	=	$\sqrt{3}lm[n^2-\frac{1}{2}(l^2+m^2)]V_{dd\sigma}$	$-2\sqrt{3}lmn^2V_{dd\pi}$	$\frac{\sqrt{3}}{2}lm(1+n^2)V_{dd\delta}$
$E_{yz,3z^2-r^2}$	=	$\sqrt{3}mn[n^2-\frac{1}{2}(l^2+m^2)]V_{dd\sigma}$	$+\sqrt{3}mn(l^2+m^2-n^2)V_{dd\pi}$	$-\frac{\sqrt{3}}{2}mn(l^2+m^2)V_{dd\delta}$
$E_{zx,3z^2-r^2}$	=	$\sqrt{3}ln[n^2-\frac{1}{2}(l^2+m^2)]V_{dd\sigma}$	$+\sqrt{3}ln(l^2+m^2-n^2)V_{dd\pi}$	$-\frac{\sqrt{3}}{2}ln(l^2+m^2)V_{dd\delta}$
$E_{x^2-y^2,x^2-y^2}$	=	$\frac{3}{4}(l^2-m^2)^2V_{dd\sigma}$	$+[l^2+m^2-(l^2-m^2)^2]V_{dd\pi}$	$+[n^2+\frac{1}{4}(l^2-m^2)^2]V_{dd\delta}$
$E_{x^2-y^2,3z^2-r^2}$	=	$\frac{\sqrt{3}}{2}(l^2-m^2)[n^2-\frac{1}{2}(l^2+m^2)]V_{dd\sigma}$	$+\sqrt{3}n^2(m^2-l^2)V_{dd\pi}$	$+\frac{1}{4}\sqrt{3}(1+n^2)(l^2-m^2)V_{dd\delta}$
$E_{3z^2-r^2,3z^2-r^2}$	=	$[n^2-\frac{1}{2}(l^2+m^2)]^2V_{dd\sigma}$	$+3n^2(l^2+m^2)V_{dd\pi}$	$\frac{3}{4}(l^2+m^2)^2V_{dd\delta}$

B.4 Gaunt coefficients and Coulomb integrals

For the d shell, in the basis of spherical harmonics, the coefficients $G_k(m,m') = \langle lm|Y^k_q|lm'\rangle$ with $k = 2, 4$ are:

$$G_2 = \frac{1}{7\sqrt{4\pi}} \begin{bmatrix} -\sqrt{20} & \sqrt{30} & -\sqrt{20} & 0 & 0 \\ -\sqrt{30} & \sqrt{5} & \sqrt{5} & -\sqrt{30} & 0 \\ -\sqrt{20} & -\sqrt{5} & \sqrt{20} & -\sqrt{5} & -\sqrt{20} \\ 0 & -\sqrt{30} & \sqrt{5} & \sqrt{5} & -\sqrt{30} \\ 0 & 0 & -\sqrt{20} & \sqrt{30} & -\sqrt{20} \end{bmatrix}$$

$$G_4 = \frac{1}{7\sqrt{4\pi}} \begin{bmatrix} 1 & -\sqrt{5} & \sqrt{15} & -\sqrt{35} & \sqrt{70} \\ \sqrt{5} & -4 & \sqrt{30} & -\sqrt{40} & \sqrt{35} \\ \sqrt{15} & -\sqrt{30} & 6 & -\sqrt{30} & \sqrt{15} \\ \sqrt{35} & -\sqrt{40} & \sqrt{30} & -4 & \sqrt{5} \\ \sqrt{70} & -\sqrt{35} & \sqrt{15} & -\sqrt{5} & 1 \end{bmatrix}.$$

The two-index Coulomb integrals can be written as

$$\begin{aligned} U_{m,m'} &= \sum_{k=0}^{2l} a_k(mm,m'm')F_k = \sum_{k=0}^{2l} b_k(m,m')F_k, \\ J_{m,m'} &= \sum_{k=0}^{2l} a_k(mm',m'm)F_k = \sum_{k=0}^{2l} c_k(m,m')F_k, \end{aligned}$$

where

$$a_k(m_\alpha m'_\alpha, m_\beta m'_\beta) = \frac{4\pi}{2k+1} \sum_{q=-k}^{k} \langle lm_\alpha|Y^k_q|lm'_\alpha\rangle \langle lm_\beta|\overline{Y}^k_q|lm'_\beta\rangle.$$

For $l = 2$, in the basis of spherical harmonics

$$b_0 = \begin{bmatrix} 1 & 1 & 1 & 1 & 1 \\ 1 & 1 & 1 & 1 & 1 \\ 1 & 1 & 1 & 1 & 1 \\ 1 & 1 & 1 & 1 & 1 \\ 1 & 1 & 1 & 1 & 1 \end{bmatrix} \qquad b_2 = \frac{1}{49} \begin{bmatrix} 4 & -2 & -4 & -2 & 4 \\ -2 & 1 & 2 & 1 & -2 \\ -4 & 2 & 4 & 2 & -4 \\ -2 & 1 & 2 & 1 & -2 \\ 4 & -2 & -4 & -2 & 4 \end{bmatrix} \qquad b_4 = \frac{1}{49}\frac{1}{9} \begin{bmatrix} 1 & -4 & 6 & -4 & 1 \\ -4 & 16 & -24 & 16 & -4 \\ 6 & -24 & 36 & -24 & 6 \\ -4 & 16 & -24 & 16 & -4 \\ 1 & -4 & 6 & -4 & 1 \end{bmatrix}$$

$$c_0 = \begin{bmatrix} 1 & 0 & 0 & 0 & 0 \\ 0 & 1 & 0 & 0 & 0 \\ 0 & 0 & 1 & 0 & 0 \\ 0 & 0 & 0 & 1 & 0 \\ 0 & 0 & 0 & 0 & 1 \end{bmatrix} \qquad c_2 = \frac{1}{49} \begin{bmatrix} 4 & 6 & 4 & 0 & 0 \\ 6 & 1 & 1 & 6 & 0 \\ 4 & 1 & 4 & 1 & 4 \\ 0 & 6 & 1 & 1 & 6 \\ 0 & 0 & 4 & 6 & 4 \end{bmatrix} \qquad c_4 = \frac{1}{49}\frac{1}{9} \begin{bmatrix} 1 & 5 & 15 & 35 & 70 \\ 5 & 16 & 30 & 40 & 35 \\ 15 & 30 & 36 & 30 & 15 \\ 35 & 40 & 30 & 16 & 5 \\ 70 & 35 & 15 & 5 & 1 \end{bmatrix}$$

In the basis of real harmonics, we find instead

$$b_0 = \begin{bmatrix} 1 & 1 & 1 & 1 & 1 \\ 1 & 1 & 1 & 1 & 1 \\ 1 & 1 & 1 & 1 & 1 \\ 1 & 1 & 1 & 1 & 1 \\ 1 & 1 & 1 & 1 & 1 \end{bmatrix} \quad b_2 = \frac{1}{49} \begin{bmatrix} 4 & -2 & -4 & -2 & 4 \\ -2 & 4 & 2 & -2 & -2 \\ -4 & 2 & 4 & 2 & -4 \\ -2 & -2 & 2 & 4 & -2 \\ 4 & -2 & -4 & -2 & 4 \end{bmatrix} \quad b_4 = \frac{1}{49}\frac{1}{9} \begin{bmatrix} 36 & -4 & 6 & -4 & -34 \\ -4 & 36 & -24 & -4 & -4 \\ 6 & -24 & 36 & -24 & 6 \\ -4 & -4 & -24 & 36 & -4 \\ -34 & -4 & 6 & -4 & 36 \end{bmatrix}$$

$$c_0 = \begin{bmatrix} 1 & 0 & 0 & 0 & 0 \\ 0 & 1 & 0 & 0 & 0 \\ 0 & 0 & 1 & 0 & 0 \\ 0 & 0 & 0 & 1 & 0 \\ 0 & 0 & 0 & 0 & 1 \end{bmatrix} \quad c_2 = \frac{1}{49} \begin{bmatrix} 4 & 3 & 4 & 3 & 0 \\ 3 & 4 & 1 & 3 & 3 \\ 4 & 1 & 4 & 1 & 4 \\ 3 & 3 & 1 & 4 & 3 \\ 0 & 3 & 4 & 3 & 4 \end{bmatrix} \quad c_4 = \frac{1}{49}\frac{1}{9} \begin{bmatrix} 36 & 20 & 15 & 20 & 35 \\ 20 & 36 & 30 & 20 & 20 \\ 15 & 30 & 36 & 30 & 15 \\ 20 & 20 & 30 & 36 & 20 \\ 35 & 20 & 15 & 20 & 36 \end{bmatrix}$$

For $l = 2$ the transformation matrix M from spherical to real harmonics is

$$M = \frac{1}{\sqrt{2}} \begin{bmatrix} -i & 0 & 0 & 0 & i \\ 0 & i & 0 & i & 0 \\ 0 & 0 & \sqrt{2} & 0 & 0 \\ 0 & -1 & 0 & 1 & 0 \\ 1 & 0 & 0 & 0 & 1 \end{bmatrix}.$$

Sometimes the Coulomb integrals are given as linear combination of Racah parameters instead than of Slater integrals F_k. For the d shell, the Racah parameters are $A = F_0 - \frac{49}{441}F_4$, $B = \frac{1}{49}F_2 - \frac{5}{441}F_4$, and $C = \frac{35}{441}F_4$.

References

[1] W. Kohn, *Nobel Lecture: Electronic structure of matterwave functions and density functionals*, Rev. Mod. Phys. **71**, 1253 (1998)

[2] U. von Barth, Physica Scripta **109**, 9 (2004)

[3] R.M. Martin, *Electronic Structure, Basic Theory and Practical Methods* (Cambridge University Press, 2004)

[4] E. Pavarini, E. Koch and A.I. Lichtenstein, Phys. Rev. Lett. **101**, 266405 (2008)

[5] W. Metzner and D. Vollhardt, Phys. Rev. Lett. **62**, 324327 (1989)
A. Georges and G. Kotliar, Phys. Rev. B **45**, 6479 (1992)

[6] A.C. Hewson, *The Kondo problem to heavy Fermions* (Cambridge University Press, 1993)

[7] J.E. Hirsch and R.M. Fye, Phys. Rev. Lett. **56**, 2521 (1986)

[8] E. Gull, A.J. Millis, A.I. Lichtenstein, A.N. Rubtsov, M. Troyer and P. Werner, Rev. Mod. Phys. **83**, 349 (2011)

[9] M. Caffarel, W. Krauth, Phys. Rev. Lett. **72**, 1545 (1994)
E. Koch, G. Sangiovanni, and O. Gunnarsson, Phys. Rev. B **78**, 115102 (2008)

[10] A. Georges, G. Kotliar, W. Krauth, and M.J. Rozenberg, Rev. Mod. Phys. **68**, 13 (1996)

[11] O. Gunnarsson, Phys. Rev. B **41**, 514 (1990)

[12] E. Pavarini, A. Yamasaki, J. Nuss and O.K. Andersen, New J. Phys. **7**, 188 (2005)

[13] N. Marzari and D. Vanderbilt, Phys. Rev. B **56**, 12847 (1997)

[14] B. Amadon, F. Lechermann, A. Georges, F. Jollet, T.O. Wehling, and A.I. Lichtenstein, Phys. Rev. B **77**, 205112 (2008)

[15] V.I. Anisimov, F. Aryasetiawan and A.I. Lichtenstein, J. Phys. Cond. Mat. **9**, 767 (1997)

[16] O. Gunnarsson, O.K. Andersen, O. Jepsen and J. Zaanen, Phys. Rev. B **37**, 1708 (1989)

[17] F. Aryasetiawan, M. Imada, A. Georges, G. Koliar, S. Biermann, and A.I. Lichtenstein, Phys. Rev. B **70**, 195104 (2004)

[18] V.I. Anisimov, A.I. Poteryaev, M.A. Korotin, A.O. Anokhin, and G. Kotliar, J. Phys: Condens. Matter **9**, 7359 (1997)
A.I. Lichtenstein and M.I. Katsnelson, Phys. Rev. B **57**, 6884 (1998)

[19] A. Georges, in *Lectures on the Physics of Highly Correlated Electron Systems VIII*, American Institute of Physics Conference Proceedings **715**, 3 (2004)

[20] M. Imada and T. Miyake, J. Phys. Soc. Jpn. **79**, 112001 (2010)

[21] G. Kotliar, S.Y. Savrasov, K. Haule, V.S. Oudovenko, O. Parcollet and C.A. Marianetti, Rev. Mod. Phys. **78**, 865 (2006)

[22] E. Gorelov, M. Karolak, T. O. Wehling, F. Lechermann, A.I. Lichtenstein and E. Pavarini, Phys. Rev. Lett. **104**, 226401 (2010)

[23] T. Maier, M. Jarrell, T. Pruschke, and M. Hettler, Rev. Mod. Phys. **77**, 1027 (2005).

[24] E. Pavarini, S. Biermann, A. Poteryaev, A.I. Lichtenstein, A. Georges and O. K. Andersen, Phys. Rev. Lett. **92**, 176403 (2004)

[25] O. Gunnarsson, E. Koch and R. Martin, Phys. Rev. B **57**, 1146 (1997)

[26] M. De Raychahudhury, E. Pavarini and O.K. Andersen, Phys. Rev. Lett. **99**, 126402 (2007)

[27] K.I. Kugel and D.I. Khomskii, Zh. Eksp. Teor. Fiz. **64**, 1429 (1973) [Sov. Phys. JETP **37**, 725 (1973)]

[28] P. Fazekas, *Lecture Notes on Electron Correlation and Magnetism* (World Scientific, Singapore, 1999)

[29] W. G. Yin, D. Volja, and W. Ku, Phys. Rev. Lett. **96**, 116405 (2006)

[30] I. Leonov, N. Binggeli, Dm. Korotin, V.I. Anisimov, and D. Vollhardt Phys. Rev. Lett. **101**, 096405 (2008); I. Leonov, Dm. Korotin, N. Binggeli, V.I. Anisimov, and D. Vollhardt Phys. Rev. B **81**, 075109 (2010)

[31] K.H. Ahn, and A.J. Millis, Phys. Rev. B **61**, 13545 (2000)

[32] A. Flesch, G. Zhang, E. Koch and E. Pavarini, arXiv:1106.2439 (2011)

[33] E. Pavarini and E. Koch, Phys. Rev. Lett. **104**, 086402 (2010)

[34] M.C. Sánchez, G. Subías, J. García, and J. Blasco, Phys. Rev. Lett. **90**, 045503 (2003)

[35] J.-S. Zhou and J.B. Goodenough, Phys. Rev. B **68**, 144406 (2003) and Phys. Rev. Lett. **96**, 247202 (2006)

[36] P.W. Anderson, Science **177**, 393 (1972)

[37] R. B. Laughlin and D. Pines, Proceedings of the National Accademy of Science **97**, 28 (2000)

[38] W. A. Harrison, *Electronic Structure and The Properties of Solids* (Dover, 1989)